Neurobiology of Stress 8 (2018) 42–56

Contents lists available at ScienceDirect

Neurobiology of Stress

journal homepage: www.elsevier.com/locate/ynstr

Chronic social stress induces peripheral and central immune activation, blunted mesolimbic dopamine function, and reduced reward-directed behaviour in mice

Giorgio Bergamini[a,h,i], Jonas Mechtersheimer[a], Damiano Azzinnari[a,i], Hannes Sigrist[a], Michaela Buerge[a,i], Robert Dallmann[b], Robert Freije[c], Afroditi Kouraki[d], Jolanta Opacka-Juffry[d], Erich Seifritz[e,i], Boris Ferger[f], Tobias Suter[g,i], Christopher R. Pryce[a,i,*]

[a] *Preclinical Laboratory for Translational Research into Affective Disorders, Department of Psychiatry, Psychotherapy and Psychosomatics, Psychiatric Hospital, University of Zurich, Switzerland*
[b] *Warwick Medical School, University of Warwick, Coventry, United Kingdom*
[c] *Brains On-line, Groningen, The Netherlands*
[d] *Department of Life Sciences, University of Roehampton, London, UK*
[e] *Department of Psychiatry, Psychotherapy and Psychosomatics, Psychiatric Hospital, University of Zurich, Switzerland*
[f] *CNS Diseases Research Germany, Boehringer Ingelheim Pharma GmbH & Co. KG., Biberach, Germany*
[g] *Neuroimmunology and MS Research, Neurology, and Clinical Research Priority Program Multiple Sclerosis, University Hospital Zurich, University of Zurich, Switzerland*
[h] *Center for Clinical Studies, Vetsuisse Faculty, University of Zurich, Switzerland*
[i] *Neuroscience Center Zurich, University of Zurich and ETH Zurich, Switzerland*

ARTICLE INFO

Keywords:
Social stress
Immune activation
Mesolimbic dopamine system
Reward
Depression
Mouse model

ABSTRACT

Psychosocial stress is a major risk factor for depression, stress leads to peripheral and central immune activation, immune activation is associated with blunted dopamine (DA) neural function, DA function underlies reward interest, and reduced reward interest is a core symptom of depression. These states might be inter-independent in a complex causal pathway. Whilst animal-model evidence exists for some specific steps in the pathway, there is currently no animal model in which it has been demonstrated that social stress leads to each of these immune, neural and behavioural states. Such a model would provide important existential evidence for the complex pathway and would enable the study of causality and mediating mechanisms at specific steps in the pathway. Therefore, in the present mouse study we investigated for effects of 15-day resident-intruder chronic social stress (CSS) on each of these states. Relative to controls, CSS mice exhibited higher spleen levels of granulocytes, inflammatory monocytes and T helper 17 cells; plasma levels of inducible nitric oxide synthase; and liver expression of genes encoding kynurenine pathway enzymes. CSS led in the ventral tegmental area to higher levels of kynurenine and the microglia markers Iba1 and *Cd11b* and higher binding activity of DA D1 receptor; and in the nucleus accumbens (NAcc) to higher kynurenine, lower DA turnover and lower *c-fos* expression. Pharmacological challenge with DA reuptake inhibitor identified attenuation of DA stimulatory effects on locomotor activity and NAcc *c-fos* expression in CSS mice. In behavioural tests of operant responding for sucrose reward validated as sensitive assays for NAcc DA function, CSS mice exhibited less reward-directed behaviour. Therefore, this mouse study demonstrates that a chronic social stressor leads to changes in each of the immune, neural and behavioural states proposed to mediate between stress and disruption of DA-dependent reward processing. The model can now be applied to investigate causality and, if demonstrated, underlying mechanisms in specific steps of this immune-neural-behavioural pathway, and thereby to identify potential therapeutic targets.

* Corresponding author. PLaTRAD, Department of Psychiatry, Psychotherapy and Psychosomatics, Psychiatric Hospital, University of Zurich, August Forel-Strasse 7, CH-8008, Zürich, Switzerland.
E-mail address: christopher.pryce@bli.uzh.ch (C.R. Pryce).

https://doi.org/10.1016/j.ynstr.2018.01.004
Received 28 November 2017; Received in revised form 19 December 2017; Accepted 31 January 2018
Available online 02 February 2018

1. Introduction

Stress-related neuropsychiatric disorders often present with psychopathology of reward processing. Depression is a prevalent example, with a core symptom being reduced interest in reward (DSM-5 2013; Pizzagalli, 2014). Within the research domain criteria (RDoC) framework, Positive valence systems is the domain that includes dimensions of reward processing (Cuthbert and Insel, 2013). Reward valuation including under effortful conditions (Sherdell et al., 2012; Treadway et al., 2012), and stimulus-reward learning and expectancy (Pizzagalli et al., 2005), are examples of positive valence dimensions that can be pathological in depression. Deficient reward processing co-occurs with reduced activation of the striatum, in particular the nucleus accumbens (NAcc) (Arrondo et al., 2015). The NAcc receives dopamine (DA) inputs from cell bodies in the ventral tegmental area (VTA) and this is a major pathway in the mesolimbic DA neural circuit of reward processing (Pizzagalli, 2014). Rodent studies have demonstrated the importance of the VTA-NAcc DA pathway in regulating reward-directed behaviour, including approach motivation, reward valuation and reward expectancy (Bergamini et al., 2016b; Russo and Nestler, 2013; Salamone et al., 2015). Whilst it is often proposed that pathology in this pathway underlies impaired reward processing in depression (Dunlop and Nemeroff, 2007; Pizzagalli, 2014), the responsible aetio-pathophysiological mechanisms are poorly understood.

Stressful environmental life events are major aetiological factors in depression, with uncontrollable psychosocial stressors conferring particularly high risk to trigger and maintain episodes (Kendler et al., 1999; Slavich et al., 2009). Animal models allow for the causal study of effects of environmental stressors on brain and behaviour. In mice, the resident-intruder paradigm is used to induce social stress and has been applied in various forms, including repeated social defeat (RSD) (Wohleb et al., 2011), chronic social defeat (CSD) (Krishnan et al., 2007) and chronic social stress (CSS) (Azzinnari et al., 2014). In these paradigms, mice are exposed to chronic, uncontrollable social stress (Azzinnari et al., 2014; Kudryavtseva et al., 1991). CSS involves placing the subject mouse with an aggressive resident mouse for a brief period of attack without injury followed by continuous distal exposure, and repeating this with a different resident across 15 days. Behavioural effects of these stressors include increased anxiety (RSD: (Wohleb et al., 2011), CSD (Krishnan et al., 2007)), increased aversion sensitivity, decreased aversion control, increased fatigue (CSS (Azzinnari et al., 2014; Fuertig et al., 2016)), decreased sensitivity to gustatory reward (CSD (Krishnan et al., 2007)), decreased effortful valuation of gustatory reward and decreased reward expectancy (CSS (Bergamini et al., 2016a)).

There is human and animal evidence that stressors activate the immune-inflammatory system, with noradrenaline released from the sympathetic branch of the autonomic nervous system binding to noradrenergic receptors on myeloid cells in the spleen and other immune tissues being a major brain-periphery mediator (Bierhaus et al., 2003; Johnson et al., 2005; Wohleb et al., 2011). In healthy humans, acute psychosocial stress increases blood levels of proinflammatory chemokines and cytokines (Bierhaus et al., 2003). Chronic social stress is associated with increased blood levels of C-reactive protein (CRP), interleukin (IL)-6 and soluble receptor for tumor necrosis factor-α (TNF-α) (Chiang et al., 2012; Gruenewald et al., 2009), and is proposed to lead to low-grade systemic inflammation (Rohleder, 2014). Turning to depression, there is substantive evidence for immune activation, including higher blood levels of inflammatory markers such as CRP, IL-6, IL-1 and TNF-α (Dowlati et al., 2010) and also of T-cell activation markers (Maes, 2010). One down-stream effect of higher proinflammatory cytokines is activation of the kynurenine pathway of tryptophan metabolism (Campbell et al., 2014; Haroon et al., 2012; Schwarcz et al., 2012), for which there is also evidence in depression (Savitz et al., 2015a, 2015b; Steiner et al., 2011; Sublette et al., 2011). Kynurenine metabolites include 3-hydroxykynurenine (3-HK), a free radical generator that promotes oxidative stress (Schwarcz et al., 2012), and quinolinic acid, a glutamate receptor agonist and neurotoxin (Dantzer and Walker, 2014). In mice, the stressors RSD, CSD and CSS induce higher blood levels of some proinflammatory cytokines (e.g. TNF-α, IFN-γ) and splenomegaly (Azzinnari et al., 2014; Fuertig et al., 2016; Savignac et al., 2011; Wohleb et al., 2014). Mouse CSS increases kynurenine pathway activity in the blood and in prefrontal cortex, amygdala and hippocampus (Fuertig et al., 2016), whilst RSD induces brain trafficking of myeloid cells as well as microglial activation in these same brain regions (Wohleb et al., 2011, 2013).

With regard to immune activation impacting on DA-modulated behavioural processes, in depressed patients, plasma levels of CRP and inflammatory cytokines correlated negatively with resting-state functional connectivity between ventral striatum (NAcc) and prefrontal cortex, reward sensitivity, and psychomotor function (Felger et al., 2016; Goldsmith et al., 2016). In patients treated chronically with IFN-α for hepatitis C or malignant melanoma, 50% met criteria for depression; activation of ventral striatum in response to reward was reduced, and symptoms included reduced reward sensitivity, as well as motor slowing and fatigue (Capuron et al., 2012). Acute administration of lipopolysaccharide (LPS) to healthy volunteers reduces ventral striatum response to reward (Eisenberger et al., 2010; Harrison et al., 2016). In monkeys, chronic IFN-α led to less effortful responding for sucrose and attenuated stimulated DA release in the striatum (Felger et al., 2013). In rodents, acute inflammatory challenge, e.g. IL-1β, LPS, CD40 agonist antibody, induces sickness followed by a period of reduced preference, consumption and effortful responding for sucrose (Cathomas et al., 2015; Nunes et al., 2014; Vichaya et al., 2014). These inflammatory factors induce post-sickness reduced DA synthesis and release (Kitagami et al., 2003; Reinert et al., 2014). Finally, CSD has been reported to increase VTA microglia activation and decrease NAcc DA turnover (Tanaka et al., 2012).

Given the above evidence, it would clearly be important to identify an animal model in which chronic social stress leads to the constellation of: immune-inflammatory activation in the periphery, immune activation in the VTA-NAcc DA pathway, reduced VTA-NAcc DA pathway functioning, and reduced NAcc DA-dependent reward-directed behaviour. This model could then be utilised to investigate cause-effect pathophysiological mechanisms at the various interfaces, with the aim of identifying potential targets for treatment of reward-related psychopathologies. Here we report on such a model in mice.

2. Materials and methods

2.1. Animals and housing

Breeding of C57BL/6J mice was conducted in-house. For all experiments, breeding pairs contributed either 1 or 2 offspring to the CSS and/or CON group. Male offspring were weaned at age 4 weeks and caged in groups of 2–3 littermates. Mice were aged 10–13 weeks and weighed 24.0–30.0 g at study onset. Male CD-1 mice (Janvier, Saint-Berthevin, France) were aged 8 months, were ex-breeders, and caged singly at study onset. Mice were maintained on a reversed 12:12 h light-dark cycle (lights off 07:00–19:00 h) in an individually-ventilated caging system at 21–22 °C and 50–60% humidity. Complete-pellet diet (Provimi, Kliba Ltd, Kaiseraugst, Switzerland) and water were available *ad libitum*, unless stated otherwise below for operant training and testing. All procedures were conducted during the dark phase of the cycle. The study was conducted under permits for animal experimentation (170/2012, 149/2015) issued by the Veterinary Office of canton Zurich in accordance with the regulations of the Swiss Federal Veterinary Office. All efforts were made to minimize the number of mice studied and any unnecessary stress.

2.2. Experimental design

Ten experiments were conducted with C57BL/6J male mice. Each experiment investigated the effect of CSS relative to control handling on immune cells/inflammation status or DA function or behaviour, except one experiment which provided data on immune cells and DA function from the same mice. This overall design provided data on different measures for the same brain region, and avoided any confound of procedures required for behavioural experiments on immune or DA function. The design of each experiment (Expt) is presented in Fig. S1. In each of Expts 1–9 a motor activity test in a novel arena was conducted and total activity was used to counterbalance allocation of mice to CSS and CON groups (Azzinnari et al., 2014). In Expt 1, CSS effects on spleen and whole brain immune-cell status were assessed using flow cytometry. In Expt 2, liver gene expression for kynurenine pathway enzymes was measured using qPCR, and plasma inducible nitric oxide synthase (iNOS) was measured in ELISA. In Expt 3, immunohistochemistry of the microglia marker ionized calcium-binding adapter molecule 1 (Iba1) in VTA and NAcc was conducted. In Expt 4, VTA expression of the microglia marker gene *Cd11b* and of genes encoding DA synthesis and transport proteins was measured using RT qPCR. In Expt 5, tissue level of kynurenine pathway metabolites was determined in VTA and NAcc using LC-MS/MS. In Expt 6, VTA and NAcc binding of DA D1 and D2 receptors was determined using quantitative autoradiography. In Expt 7, NAcc tissue level of DA and its major metabolites were measured using HPLC-ED. In Expt 8, CSS effects on responsiveness to DA reuptake inhibitor challenge were assessed in terms of an activity test, home-cage activity, and NAcc immediate-early gene expression. In Expt 9, reward consumption under freely available conditions was assessed using a two-bottle saccharin versus water test. In Expt 10, mice were trained in an operant apparatus with sucrose reinforcement, followed by measurement of reward-directed behaviour in operant tests.

2.3. Chronic social stress

Chronic social stress (CSS) was conducted as described in detail previously (Azzinnari et al., 2014). Briefly, the home cages of aggressive CD-1 mice were divided by a transparent, perforated divider. A CSS mouse was placed in the same compartment as the CD-1 resident mouse for either a cumulative total of 60 s physical attack or 10 min maximum, on days 1–15. Thereafter the two mice were placed one per compartment and remained in sensory contact for 24 h. To prevent bite wounds during attacks the lower incisors of CD-1 mice were trimmed every third day. The timing of attacks and limiting them to 1 min per day maximum and the trimming of the incisor teeth of CD-1 mice eliminates the deep bite wounds that otherwise occur (Golden et al., 2011), and also markedly reduces the frequency of surface wounds (Pryce and Fuchs, 2017). The number of surface wounds per experiment was 1–2 in 2–4 of 12 CSS mice, as we reported in our original description of this protocol (Azzinnari et al., 2014). The CSS – CD-1 mouse pairings were rotated so that each CSS mouse was placed in the home cage of an unfamiliar CD-1 mouse each day. Each CSS mouse displayed submissive behaviour and vocalization but continued to be attacked by the CD-1 mouse; therefore, CSS mice experienced an uncontrollable social stressor. From the last attack session on day 15 until the end of the experiment, each CSS mouse remained in the same divided cage next to the same CD-1 mouse without further attacks. Control (CON) mice remained in littermate pairs, the standard social condition in our laboratory, and were handled daily.

2.4. Flow cytometry of splenocytes and brain mononuclear cells

In Expt 1 (Fig. S1), mice were anesthetized using isoflurane inhalation, transcardially perfused with Ringer solution (Braun Medical), and spleen and brain were dissected out. For isolation of splenocytes, the spleen was minced in Roswell Park Memorial Institute (RPMI) medium (5% foetal-calf serum) and digested for 20 min at RT in Hanks' balanced salt solution (HBSS) containing 50 µg/ml DNase I and 100 µg/ml collagenase/dispase (Roche). The digested spleen was passed through a 100 µl Nylon mesh (BD Biosciences), followed by lysis of erythrocytes in ammonium-chloride-potassium (ACK) buffer. After a final resuspension in HBSS, cells were counted (using a Neubauer chamber) and 5×10^6 splenocytes were stained for each spleen. Mononuclear cells (MNCs) from entire brain were isolated as described previously (Ferretti et al., 2016; Moransard et al., 2010): the brain was chopped with a scalpel, and digested for 30 min at 37 °C in HBSS containing 50 µg/ml DNase I and 100 µg/ml collagenase/dispase (Roche). The digested brain was passed through a 100 µl Nylon mesh, pelleted and re-suspended in 30% Percoll (Sigma) in HBSS. Myelin debris was removed via aspiration. The gradient was centrifuged at 29,000 g for 30 min at 4 °C. The interphase containing MNCs was collected and washed with HBSS.

For flow cytometry of splenocytes and brain MNCs, each sample was divided into two halves: one aliquot was used for extracellular staining and the other for extracellular + intracellular staining. Intracellular staining of cytokines was performed after a 4 h incubation with phorbol myristate acetate (PMA, 50 ng/ml) and ionomycin (500 ng/mL). Flow cytometry was conducted with a LSR II Fortessa (BD). Cells were re-suspended in FACS buffer comprising 2% FCS, 10 mM EDTA and 0.01% NaN_3 in PBS. Fc receptors were blocked by incubation with anti-mouse CD16/32 (BioLegend). The LIVE/DEAD® Fixable Aqua Dead Cell Stain Kit (Molecular Probes) was used to exclude non-viable cells. For extracellular staining, the antibodies used were: CD45 (BD Biosciences), CD11b (BD Biosciences), MHC II (BD Biosciences) and Ly6c (Biolegend). For extracellular + intracellular staining, the antibodies used were: CD45, CD11b, CD4 (Biolegend), Foxp3 (eBioscience), IL-17A (BD Biosciences), CD8 (eBioscience), TNF-α (BD Biosciences) and IFN-γ (BD Biosciences). Splenic immune cells were counted using a Neubauer chamber, and the same number of cells per mouse was used for analysis. For counts of brain MNCs, fluorescent Counting Beads were used (Molecular Probes). Expression levels of proteins were estimated using the geometric mean of fluorescence intensity (MFI). FlowJo software (Tree Star) was used for flow cytometry data analysis.

2.5. ELISA for plasma inducible nitric oxide synthase (iNOS)

In Expt 2 (Fig. S1), mice were decapitated and trunk blood was collected into EDTA-coated tubes (Microvette 500 K3E, Sarstedt) and placed on ice. Tubes were centrifuged at 3000 rpm for 15 min at 4 °C and plasma aliquots were transferred to Protein LoBind tubes (Eppendorf) and stored at −80 °C. Plasma iNOS was measured in duplicate using a commercial ELISA kit (Mouse Inducible nitric oxide synthase ELISA Kit, MyBioSource) according to the manufacturer's instructions.

2.6. Iba1 immunoperoxidase staining

In Expt 3 (Fig. S1), mice were deeply anesthetized with pentobarbital and perfused transcardially with phosphate-buffered saline (PBS, pH 7.4) and fixative (4% paraformaldehyde (PFA) in PBS). Brains were dissected out, post-fixed overnight (o/n) in 4% PFA and cryoprotected in 30% sucrose for 48 h, frozen on powdered dry ice and stored at −80 °C until sectioning. Brains were sectioned coronally at 40 µm using a microtome (Zeiss), with sections collected in antifreeze solution (15% glucose and 30% ethylene glycol in 50 mM phosphate buffer, pH 7.4) and stored at −20 °C. Sections including the VTA (bregma −2.8 to −3.0 mm) or NAcc (bregma 1.1–1.5 mm), 3–6 per region/mouse, were identified referring to a mouse brain atlas (Franklin and Paxinos, 2008). Free-floating sections were washed with PBS, quenched with 3% H_2O_2 for 15 min, blocked with 10% normal serum and incubated o/n at 4 °C with a rabbit anti-Iba1 antibody (1:1000; Wako Chemicals) followed by a 2 h RT incubation with a

biotinylated goat anti-rabbit secondary antibody (1:500; Millipore). Sections were then incubated with 1% avidin-biotin peroxidase complex (Vectastain ABC kit, Vector) for 30 min at RT. Labeling was visualized using diaminobenzidine (DAB) solution. Images were acquired using a brightfield microscope (Axiovert, Zeiss). Digital image analysis (DIA) of Iba1 staining was conducted blind with respect to mouse identity using the software ImageJ (NIH): the threshold for positive staining was determined and used to calculate the percentage of the area of each image that was Iba1-immunoreactive (IR) (Klaus et al., 2016; Wohleb et al., 2011).

2.7. Real-time quantitative PCR (qPCR)

Mice were decapitated, and liver (Expt 2) or brain (Expt 4, Expt 8) (Fig. S1) was dissected out and frozen on dry ice. For liver, total RNA was isolated using Trizol (Ambion) according to the manufacturer's instructions, and further digested with DNase I (Fermentas). Frozen brains were sectioned coronally at 1.0 mm intervals using a stainless-steel brain matrix, and the VTA (−2.5 to −3.5 ± 0.2 mm) or NAcc (bregma 1.8 to 0.8 ± 0.2 mm) was identified referring to a mouse brain atlas (Franklin and Paxinos, 2008) and microdissected bilaterally using a brain punch (∅ = 0.5 mm for VTA and ∅ = 1.0 mm for NAcc) (Azzinnari et al., 2014). Tissue biopsies per region were combined and placed in 350 µl lysis RLT buffer (Qiagen) containing 1% β-mercaptoethanol, and homogenized using a tissue lyser (Mixer-Mill 300, Qiagen) with stainless steel beads (∅ = 5 mm, Retsch). Total RNA was isolated using the RNeasy Plus Micro Kit (Qiagen). The genes of interest and the respective primers used are given in Table S1. RNA was reverse transcribed using the High Capacity cDNA Reverse Transcription Kit (Applied Biosystems). Quantitative gene expression analysis was performed using SYBR green (Applied Biosystems) and a 7900HT Fast Real-Time PCR System (Applied Biosystems). PCR cycle conditions were: 2 min at 50 °C, 2 min at 95 °C; 40 cycles: 15 s at 95 °C, 30 s at 60 °C, 30 s at 72 °C. A melting curve was run for each PCR plate. Threshold cycle (Ct) values of the target gene were normalized to the Ct values of the corresponding reference gene, using the ΔΔCt method (Pfaffl et al., 2002). For liver genes the geometric mean of Ct values for *Hprt1* and *Tbp* was used as the normalization factor (NF), and for brain genes *Actb* was used as the reference gene. Relative expression values were log2-transformed for statistical analysis.

2.8. LC-MS/MS of the kynurenine pathway in NAcc and VTA

In Expt 5 (Fig. S1), mice were anesthetized and transcardially perfused with saline, decapitated, and the brain dissected out, frozen on powdered dry-ice and stored at −80 °C. Frozen brains were sectioned coronally at 1.0 mm intervals and the VTA and NAcc were microdissected bilaterally. Tissue biopsies per region were combined, weighed and stored at −80 °C pre- and post-transport and transported on dry ice. Brain levels of tryptophan (TRP), kynurenine (KYN) and 3-hydroxykynurenine (3-HK), 3-hydroxyanthranilic acid (3-OH-AA) and quinolinic acid (QUIN) were measured by Brains Online using liquid chromatography (LC) tandem mass spectrometry (MS/MS). Tissue levels of 3-OH-AA and QUIN were below the lower limit of quantification (LLOQ) for all samples in both brain regions. Protein content of tissue punches was measured using the Bradford method. Brain concentrations of TRP, KYN and 3-HK are expressed as nmol or pmol/mg protein. Absolute concentrations and the KYN/TRP ratio were calculated.

2.9. Dopamine receptor autoradiography

In Expt 6 (Fig. S1), mice were decapitated and the brains dissected out, frozen on powdered dry ice, stored at −80 °C pre- and post-transport and transported on dry ice. Frozen brains were sectioned coronally at 20 µm and serial sections containing the VTA (bregma level −3.0 mm) or NAcc (bregma 1.8 mm) were collected and mounted on polysine coated slides, and stored at −80 °C prior to autoradiography; for each region, two sections were used per mouse and receptor. Autoradiography for D1 receptor binding was conducted according to (Dalton and Zavitsanou, 2011). Briefly, sections were preincubated in 0.05 M Tris-HCl buffer (pH 7.4) for 10 min, and then incubated for 1 h with 1 nM [^{3}H]SCH-23390 (spec. act. 60 Ci/mmol, 1 mCi/ml, PerkinElmer, U.S.A.) in Tris-buffer at room temperature. Non-specific binding was assessed in the presence of 1 µM unlabelled R(+)-SCH-23390 (Sigma Aldrich, U.K.). Slides were rinsed 2x in ice-cold Tris buffer. The method used for D2 receptor autoradiography is described in (Leventopoulos et al., 2009). Briefly, sections were pre-incubated in 0.05 M Tris-HCl buffer (pH 7.6) for 20 min, and then incubated for 1.5 h with 2 nM [methoxy-^{3}H]raclopride (spec. act. 85 Ci/mmol, 1 mCi/ml, American Radiolabeled Chemicals, Inc., U.S.A.) in Tris-buffer at room temperature. Non-specific binding was assessed using 1 µM unlabelled raclopride (Sigma Aldrich, U.K.). For D1 and D2 receptors, air-dried brain sections and ^{3}H-microscale standards (Amersham Biosciences) were apposed to tritium-sensitive BioMax MR hyperfilm (Kodak, U.K.) for 6 weeks to generate autoradiograms, and tissue radioactivity was then quantified by densitometry using an image analysis system (MCID™, Version 7.0, Imaging Research Inc., Interfocus Ltd, Linton, U.K.). Flat-field correction and calibration of tritium standards were applied to quantify tissue radioactivity in nCi/mg. VTA and NAcc regions of interest were sampled in both the right and left hemispheres in each section and the mean value per mouse was used for statistical analysis; imperfect images with signs of tissue damage were excluded from the analysis.

2.10. HPLC-ED of NAcc tissue dopamine and metabolites

In Expt 7 (Fig. S1), mice were decapitated and the brain dissected out, frozen on powdered dry ice and stored at −80 °C. Frozen brains were sectioned coronally at 1.0 mm intervals and the NAcc was microdissected bilaterally. The two biopsies were combined and weighed, and homogenized using 250 µl ice-cooled perchloric acid (0.4 M). Ultrasonication was conducted for 5 s at 30% power (VibraCell, VCX130PB, Sonics and Materials), followed by centrifugation at 16,000 g for 10 min at 4 °C. The supernatant was passed through a 0.22 µm filter (Minisart RC4, Sartorius AG) and kept on ice until analysis. High performance liquid chromatography (HPLC) and electrochemical detection (ED) were conducted for DA and its major metabolites dihydroxyphenylacetic acid (DOPAC) and homovanillic acid (HVA), according to (Oeckl et al., 2012). Briefly, isocratic separation of DA was carried out with a reversed-phase C18 column (YMC-Pack ODS-AQ, 100 × 2.1 mm, S-3 µm, YMC Europe GmbH). The mobile phase consisted of 1.7 mM 1-octanesulfonic acid sodium salt, 1.0 mM $Na_2EDTA \times 2H_2O$, 8.0 mM NaCl, 100 mM $NaH_2PO_4 \times 2H_2O$ (pH 3.8), mixed with 9.3% acetonitrile; it was delivered at a flow rate of 0.4 ml/min. For ED an electrochemical cell with a glassy carbon electrode and an ISAAC Ag/AgCl reference electrode (VT-03, Antec) was used. Homogenate (20 µl) was injected onto the HPLC system using an autosampler (ASI-100T). Dopamine, DOPAC and HVA concentrations were calculated using an external standard calibration and expressed as ng/mg NAcc tissue.

2.11. Behavioural testing

2.11.1. Locomotor activity test for group allocation and after GBR 12909

In each of Expts 1–8, using an automated test apparatus (Multi Conditioning System, TSE Systems (Pryce et al., 2012)), a 15-min motor activity test in a novel arena was conducted and total activity was used to counterbalance allocation of mice to CSS and CON groups (Azzinnari et al., 2014). In Expt 8 (Fig. S1), on day 16 CSS and CON mice were injected intra-peritoneally (i.p.) with either the dopamine transporter (DAT) inhibitor GBR 12909 dihydrochloride (Sigma-Aldrich) at 6 mg/kg in physiological saline vehicle (VEH) or with VEH only. After

returning to the home cage for 30 min, mice were placed into an arena for 2 h of activity measurement. This was the same arena as used for baseline activity testing but now contained a central divider with an opening (gate) through which mice could transfer from one side of the arena to the other, to stimulate activity/exploration. The main measure of interest was total locomotor activity (arbitrary units). Mice were then returned to their home cage and activity was monitored continuously for 24 h using a passive infrared sensor located above the cage (MP Motion Sensor AMN12112, Panasonic) and connected to a RedLab recording unit (1024HLS, Meilhaus Electronic). During home cage activity monitoring, CON mice were separated from their cage mate using the same dividers used to separate CSS and CD-1 mice; CON mice were habituated to the divider for 2 h per day on days 13–14. On day 17, after completion of the home-cage activity monitoring, mice were injected with a second i.p. dose of GBR 12909 or VEH (same dose as on day 16) and after 30 min were decapitated and brains were processed for NAcc RNA extraction (see Quantitative PCR assays).

2.11.2. Two-bottle saccharin test

In Expt 9 (Fig. S1), mice were habituated to 15 ml capped polypropylene tubes from which the tip had been removed to enable drinking (Cathomas et al., 2015). Two such tubes were attached adjacently to the cage lid each day at 08:00 h and removed at 16:00 h. Amount drunk per tube was calculated based on weight. Since CON mice were pair-housed, the liquid consumption per tube and cage was calculated and adjusted for individual body weights, to obtain estimated values for each mouse. On days −12 to −8 (baseline), mice were presented with one tube containing water and one tube containing 0.15% (W/V) saccharin (as sodium salt hydrate, Sigma) solution, with the left-right positioning of the two tubes alternated across days (Cathomas et al., 2015). On the final day of baseline measurements, average saccharin consumption per mouse was 5.4 ± 1.4 g, average water consumption was 0.15 ± 0.10 g, and average saccharin preference was 98.7 ± 0.5% (mean ± SD). The effects of CSS on saccharin and water drinking and saccharin preference were tested in a single test at day 16, between 08:00–16:00 h.

2.11.3. Operant reward tests

2.11.3.1. Operant apparatus. In Expt 10 (Fig. S1), training and testing were conducted using operant chambers (TSE Systems) details of which are given elsewhere (Bergamini et al., 2016a, 2016b; Ineichen et al., 2012). Briefly, nose-poke apertures detected mouse operant responses via an infra-red beam; the position of the apertures relative to the feeder port and the number of apertures used changed according to the test (see below). Sucrose pellets (14 mg, Dustless Precision Pellets, BioServ) were delivered singly into the feeder port, signalled by a tone from a speaker. Pellet retrieval was detected via infra-red beam.

2.11.3.2. Feeding protocols. Mice had *ad libitum* access to food until age 12 weeks. At week 11, for 5 days, daily body weight (BW) and daily food intake were measured to obtain mean free-feeding (baseline) values. Beginning at week 12 and continuing throughout operant training, mice were food restricted to 90–95% of baseline BW to ensure adequate motivation during operant training with sucrose pellet reinforcement. For one week prior to and throughout the 15-day CSS, mice were provided with sufficient standard diet to return to and maintain 100% of baseline BW. As described previously, CSS mice require more standard diet per day than CON mice to maintain this target BW (Bergamini et al., 2016a). Post-CSS, for the learned non-reward test (see below), mice were maintained at 95% baseline BW with CSS mice again required more standard diet than CON mice. Standard diet was provided in the home cage 2–3 h after operant training/testing and was always fully consumed within the dark phase, such that mice did not eat for about 12 h prior to operant testing.

2.11.3.3. Fixed-ratio 1 schedule of reinforcement (FR1) test and learned non-reward (LNR) test. The fixed-ratio 1 schedule of reinforcement (FR1) test is a precursor test to the learned non-reward (LNR) test, and the LNR test was used because it is sensitive to NAcc DA function, as demonstrated by the effects of pharmacological depletion of NAcc DA using 6-hydroxydopamine (Bergamini et al., 2016b). The same operant training was required for both tests. Through a series of conditioning steps mice learned to: make an operant response (nosepoke) into the feeder (trial initiation). This led to illumination of a stimulus aperture in the opposite, stimulus wall; an operant response (nosepoke) into the stimulus aperture (stimulus response) led to a 1-s tone and simultaneous delivery of one sucrose pellet into the feeder; the mouse returned to the feeder wall and retrieved the pellet (collect pellet latency), which initiated a 2.5 s time out, after which the next trial could be initiated. At the final training stage, mice had 10 s maximum for each trial initiation and 6 s maximum for each stimulus response; omission of either response resulted in a 5 s timeout prior to the next trial. A session comprised either 70 trials or 30 min, whichever occurred first. The criterion for training completion was 2 sessions of 70 trials in which ≥49 pellets were obtained. Thereafter two further daily sessions were conducted, and the mean number of pellets obtained in these four sessions was used to counterbalance allocation of mice to CSS and CON groups.

The FR1 test consisted of the same conditions as used at the final stage of training (Fig. S2) and was conducted at CSS day 8 with mice maintained at 100% baseline BW. Measures of interest were: omissions to initiate trials, omissions to emit stimulus responses in initiated trials, total pellets earned, and session duration. LNR testing began at day 16 and was conducted until mice had attained criterion on both test stages (see below). Across this period CSS mice were maintained in the same cage and next to the same CD-1 mouse. The LNR test was based on that described by (Nilsson et al., 2012) and applied in Bergamini et al. (2016b). The protocol was the same as used for the FR1 test except that there were now three spatial locations (left, middle, right) for apertures in the stimulus wall and two of these were in use at each test stage (Fig. S2). The first stage was a two-choice spatial discrimination (SD): following trial initiation, the mouse had to choose between two stimulus apertures whilst a blank panel occupied the third location (Fig. S2). A response in the correct stimulus aperture led to tone and sucrose pellet delivery in the feeder port and an incorrect response led to a 5 s timeout. Mice had 10 s maximum for each trial initiation and 6 s maximum for the choice response. The SD stage consisted of 70 trials divided into seven 10-trial blocks; SD learning criterion was nine correct choice responses within any 10-trial block. If a mouse did not attain criterion the SD test was repeated on the next day until criterion was attained. On the day after attaining SD criterion, the learned non-reward (LNR) stage was run: the SD correct stimulus was removed and replaced by the blank panel, the SD incorrect stimulus was now the correct stimulus, and the blank panel was replaced by the new incorrect stimulus (Fig. S2). The mouse must be sufficiently interested in reward to respond at the previously incorrect (non-rewarded) stimulus, in the absence of the possibility to perseverate at the previously correct stimulus. Number of trials, time allowed for trial initiation and choice responding, and learning criterion (9 correct choice responses within a 10-trial block) were the same as for the SD stage; if the mouse did not attain LNR test criterion the test was repeated on the next day until criterion was attained. Measures of interest for each of the SD and LNR test stages were the total number (cumulative across test days) of occurrences until attaining criterion of: omissions to initiate trials, omissions to emit choice responses in initiated trials, incorrect choice responses in initiated trials, total errors (i.e. the sum of the previous three error types), and correct choice responses in initiated trials. Mice required a total of 3–13 daily tests to attain criterion on both test stages. It is relevant that 6-hydroxydopamine NAcc DA depletion was without effect on behaviour at the SD stage and increased omissions to initiate

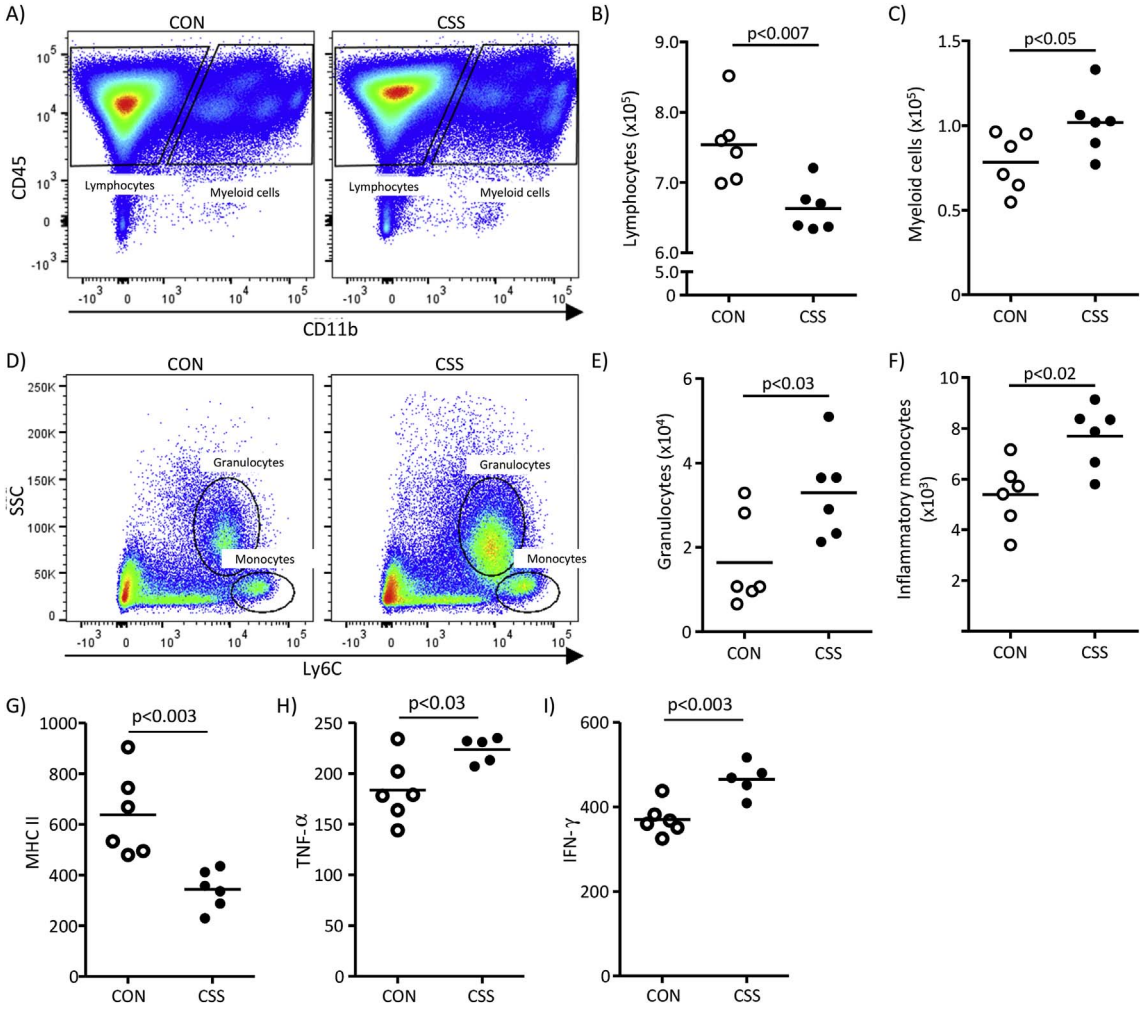

Fig. 1. Effects of CSS on splenic leukocytes at day 16 assessed using flow cytometry (Expt 1). Spleens were processed from 6 CSS and 6 CON mice. A) FACS dot plots for gating of lymphocytes and myeloid cells based on CD45 and CD11b staining, in representative CON and CSS mice. B) Cell counts for lymphocytes ($CD45^+/CD11b^-$). C) Cell counts for myeloid cells ($CD45^+/CD11b^+$). D) FACS dot plots for total myeloid cells gated based on SSC and Ly6C staining, in representative CON and CSS mice. E) Cell counts for granulocytes ($SSC^{hi}/Ly6C^{int}$). F) Cell counts for inflammatory monocytes ($SSC^{lo}/Ly6C^{hi}$). G - I) Expression levels of activation markers in splenic myeloid cells ($CD45^+/CD11b^+$); marker expression is measured as the geometric mean of fluorescence intensity (MFI). G) MHC II, H) TNF-α, I) IFN-γ. In H) and I) the data point for one CSS mouse was excluded because of a methodological problem with the intracellular staining. *p* values were obtained in unpaired *t*-tests. CD45, cluster of differentiation 45; CD11b, cluster of differentiation 11b; SSC, side scatter of cells; Ly6C, lymphocyte antigen 6C.

trials and incorrect choice responses at the LNR stage (Bergamini et al., 2016b).

2.12. Statistical analysis

Statistical analysis of CSS effects was conducted using SPSS (version 20, SPSS Inc., Chicago IL, USA). With the exception of Expt 10 an unpaired *t*-test or analysis of variance (ANOVA) was used. Where appropriate, ANOVA *post hoc* testing was conducted using the Bonferroni procedure. Analysis of covariance (ANCOVA) was used in Expt 10 (FR1 test) with % baseline body weight as covariate. Statistical significance was set at $p \leq 0.05$. Where an estimate of variance is given this is the standard deviation (SD).

3. Results

3.1. CSS induces peripheral and VTA-NAcc immune-inflammation activation

Firstly, CSS effects on spleen and whole-brain immune-cell status were investigated using flow cytometry (Fig. 1, Expt 1). For splenocytes, relative to controls, CSS mice had fewer lymphocytes ($CD45^+/CD11b^-$) ($t_{(10)} = 3.5$, $p < 0.007$, Fig. 1A and B) and more myeloid cells ($CD45^+/CD11b^+$) ($t_{(10)} = 2.3$, $p < 0.05$, Fig. 1A, C). Within the latter (Fig. 1D) both granulocytes ($SSC^{hi}/Ly6C^{int}$) ($t_{(10)} = 2.6$, $p < 0.03$, Fig. 1E) and inflammatory monocytes ($SSC^{lo}/Ly6C^{hi}$) ($t_{(10)} = 3.2$, $p < 0.02$, Fig. 1F) were more abundant in spleens of CSS than CON mice. Using mean fluorescence intensity (MFI) to quantify activation markers, major histocompatibility complex II (MHC II) surface expression on myeloid cells was lower in CSS mice ($t_{(10)} = 3.9$, $p < 0.003$, Fig. 1G). As revealed by intracellular staining and MFI, myeloid-cell expression of TNF-α ($t_{(9)} = 2.7$, $p < 0.03$, Fig. 1H) and IFN-γ ($t_{(9)} = 4.0$, $p < 0.003$, Fig. 1I) was higher in CSS than CON mice. As stated above, CSS mice had less splenic lymphocytes than CON mice: in terms of T-cell type (Fig. 2A), CSS had no effect on total numbers of $CD4^+$ T cells ($p = 0.26$, Fig. 2B) or cytotoxic $CD8^+$ T cells ($p = 0.79$, Fig. 2C). Within $CD4^+$ T cells there was no CSS effect on number of Th1 cells ($CD4^+/IFN\text{-}\gamma^+$) ($p = 0.41$, Fig. S3A and B) or Treg cells ($CD4^+/Foxp3^+$) ($p = 0.53$, Figs. S3C and D). However, CSS mice had more Th17 cells ($CD4^+/IL17A^+$) than CON mice ($t_{(9)} = 3.8$, $p < 0.005$, Fig. 2D and E). Given that the reduced total lymphocyte count in CSS mice was not accounted for by an overall reduction in T cell populations, future studies will need to investigate B cell populations.

We next investigated CSS effects on liver expression of genes

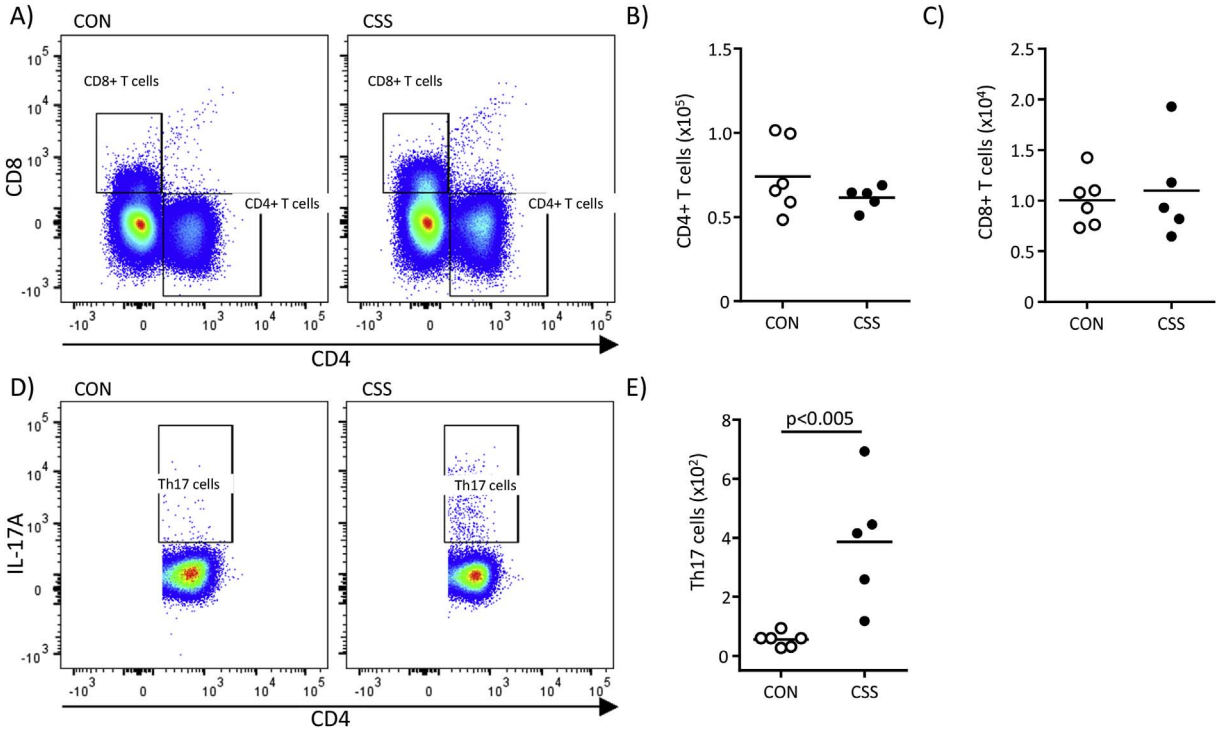

Fig. 2. Effects of CSS on splenic T cells at day 16 assessed using flow cytometry (Expt 1). Spleens were processed from 6 CSS and 6 CON mice (same mice as in Fig. 1). A) FACS dot plots for gating of $CD4^+$ and $CD8^+$ T cells in representative CON and CSS mice. B) Cell counts for $CD4^+$ T cells. C) Cell counts for $CD8^+$ T cells. D) FACS dot plots for gating of Th17 cells ($CD4^+$/IL-$17A^+$) in representative CON and CSS mice. E) Cell counts for Th17 cells. In B), C) and E) the data point for one CSS mouse was excluded because of a methodological problem with the intracellular staining. *p* value was obtained in an unpaired *t*-test. CD4, CD8, cluster of differentiation 4, 8; IL-17A, interleukin-17A; Th17, T helper 17.

encoding enzymes in the kynurenine (KYN) pathway of tryptophan catabolism (Fig. 3A) using qPCR (Fig. S1, Expt 2). CSS mice had higher liver expression of *Tdo1* ($t_{(10)} = 2.4$, $p < 0.04$), *Ido2* ($t_{(10)} = 2.6$, $p < 0.03$), *Tdo2* ($t_{(10)} = 2.6$, $p < 0.03$), *Kynu* ($t_{(10)} = 2.3$, $p < 0.05$) and *3-Haao* ($t_{(10)} = 3.4$, $p < 0.007$), and a borderline non-significant increase in *Kmo* ($p = 0.08$) (Fig. 3B). As expected, liver expression of *Ido1* was barely detectable in both CON and CSS mice i.e. Ct > 36–37 (Dai and Zhu, 2010; Fuertig et al., 2016). Given that activated myeloid cells (Expt 1) and up-regulation of the KYN pathway (Expt 2) are both associated with increased oxidative stress, we measured blood plasma levels of iNOS in the latter mice using ELISA (Expt 2): plasma iNOS was increased in CSS compared to CON mice ($t_{(10)} = 2.6$, $p < 0.03$) (Fig. 3C).

Regarding CSS effects on brain immune status, in the same mice used to study spleen leukocytes (Fig. S1, Expt 1), we isolated and analysed mononuclear cells from whole brain. There was no CSS effect on total numbers of microglia ($CD11b^+/CD45^{int}$) ($p = 0.55$, Fig. 4A and B), infiltrating myeloid cells ($CD11b^+/CD45^{hi}$) ($p = 0.70$, Fig. 4A, C), or lymphocytes ($CD11b^-/CD45^+$) ($p = 0.13$, data not shown). To assess brain region-specific effects of CSS on microglia, we quantified microglia marker Iba1 expression in the VTA and NAcc (Fig. S1, Expt 3). In the VTA a higher % area was Iba1-immunoreactive in CSS compared with CON mice ($t_{(13)} = -2.8$, $p < 0.02$, Fig. 4D and E). There was no effect of CSS on Iba1 staining in the NAcc (CON 1.55% ± 0.34%, CSS 1.52% ± 0.25%, $p = 0.82$; data not shown). In the next experiment (Fig. S1, Expt 4) the VTA was microdissected and mRNA expression of the microglia/macrophage marker *Cd11b* was measured using qPCR: CSS mice had higher VTA *Cd11b* expression than

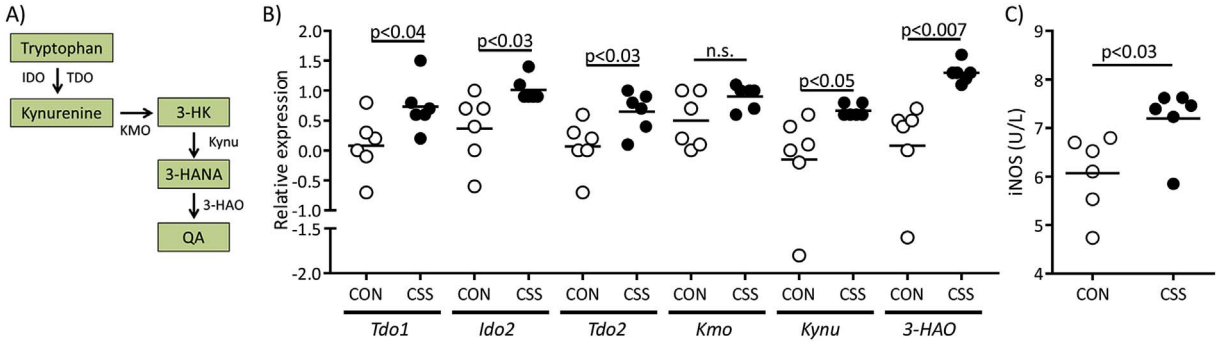

Fig. 3. Effects of CSS on liver kynurenine-pathway enzyme gene expression and on plasma iNOS levels at day 16 (Expt 2). Liver and blood-plasma were obtained from 6 CSS and 6 CON mice. A) Metabolic steps in the kynurenine (KYN) pathway showing enzymes measured: tryptophan metabolism to N-formylkynurenine is catalysed by indoleamine 2,3-dioxygenase 1 and 2 (IDO1, IDO2) and tryptophan 2,3-dioxygenase 1 and 2 (TDO1, TDO2), and N-formylkynurenine is degraded by formamidase to kynurenine (KYN). KYN conversion to 3-hydroxykynurenine (3-HK) is catalysed by kynurenine 3-monooxygenase (KMO), and 3-HK to 3-hydroxyanthranilic acid (3-HANA) by kynureninase (KYNU). 3-hydroxyanthranilic acid 3,4-dioxygenase (3-HAO) converts 3-HANA to 2-amino-3-carboxymuconic-6-semialdehyde, which rearranges to form quinolinic acid (QA). B) Comparison of liver mRNA expression of the gene encoding each of the above enzymes, as measured using qPCR, in CON and CSS mice. C) Plasma concentration (International Units per litre plasma) of inducible nitric oxide synthase measured using ELISA. *p* values were obtained in unpaired *t*-tests.

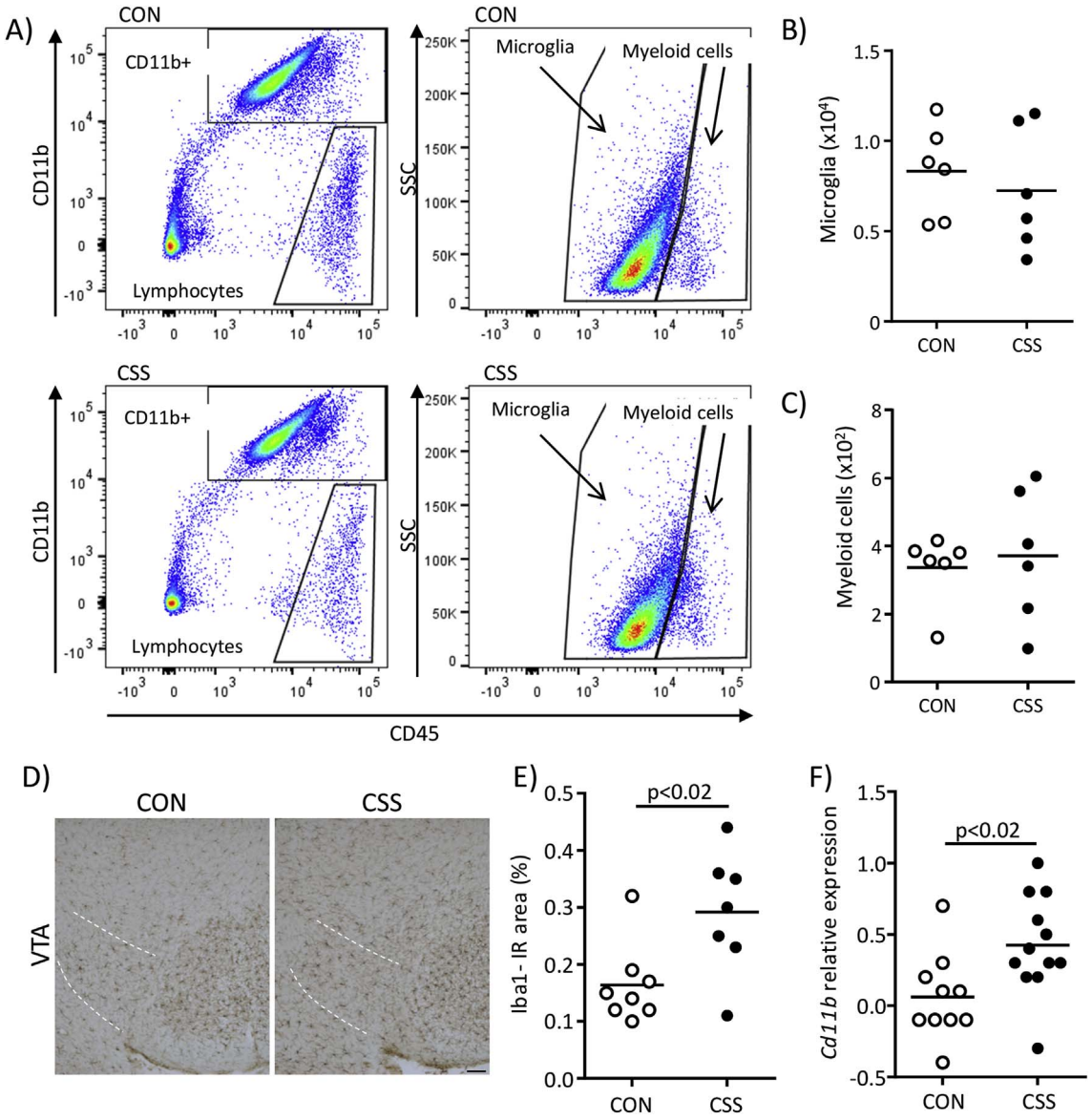

Fig. 4. Effects of CSS on brain measures of immune status at day 16 (Expts 1, 3 and 4). Expt 1: Fresh brains were obtained from 6 CSS and 6 CON mice (same mice as in Figs. 1 and 2). A) FACS dot plots from representative CON and CSS mice for mononuclear cells from whole brain tissue showing gating of lymphocytes ($CD11b^-/CD45^+$) and $CD11b^+$ cells (left-hand dot plots); within $CD11b^+$ cells, CD45 staining was used to gate microglia ($CD45^{int}$) and brain-infiltrating myeloid cells ($CD45^{hi}$) (right-hand dot plots). B) Cell counts for microglia. C) Cell counts for myeloid cells. Expt 3: Perfused brains were obtained from 7 CSS and 8 CON mice were sectioned and immunostained for the microglia marker Iba1. D) Representative images of Iba1 staining in the ventral tegmental area (VTA, demarcated with dashed white lines) from a CON mouse and a CSS mouse. E) Percentage $Iba1^+$ immunoreactive (IR) area in the VTA. Expt 4: Fresh fixed brains were obtained from 12 CSS and 10 CON mice. F) Comparison of VTA expression of *CD11b* mRNA measured using qPCR. *p* values were obtained in unpaired *t*-tests.

Table 1
Effects of CSS on the kynurenine pathway activity in VTA and NAcc.

Compound		VTA	NAcc
TRP	CON	0.86 ± 0.46	0.92 ± 0.66
(nmol/mg protein)	CSS	1.04 ± 0.6	1.46 ± 0.73#
KYN	CON	2.13 ± 0.82	2.57 ± 1.82
(pmol/mg protein)	CSS	4.03 ± 2.96#	4.76 ± 2.62*
KYN/TRP	CON	2.72 ± 0.79	3.05 ± 0.82
(*1000)	CSS	3.91 ± 1.21*	3.24 ± 0.57
3-HK	CON	1.15 ± 0.36	1.57 ± 1.38
(pmol/mg protein)	CSS	1.38 ± 0.69	2.05 ± 0.95

Concentrations are mean ± SD; VTA: CON n = 10, CSS n = 8; NAcc: CON n = 10, CSS n = 11.
*p < 0.05, #p < 0.10.

CON mice ($t_{(20)} = -2.7$, $p < 0.02$, Fig. 4F).

Building on the evidence that CSS leads to increased liver expression of KYN pathway genes, as well as previous evidence that CSS increases KYN and 3-HK levels in blood and brain (Fuertig et al., 2016), we microdissected the VTA and NAcc for determination of tryptophan (TRP), KYN and 3-HK using LC-MS/MS (Fig. S1, Expt 5): In VTA, CSS led to a trend level increase in KYN ($t_{(16)} = 1.9$, $p < 0.07$) and CSS mice had a higher KYN/TRP ratio, a marker of KYN pathway activation ($t_{(16)} = 2.5$, $p < 0.03$, Table 1). In NAcc, CSS led to a trend level increase in TRP ($t_{(19)} = 1.8$, $p < 0.09$) and to higher levels of KYN ($t_{(19)} = 2.2$, $p < 0.03$, Table 1). There was no effect of CSS on 3-HK titres in VTA ($p = 0.39$) or NAcc ($p = 0.34$) (Table 1).

3.2. CSS leads to blunted functioning of the mesolimbic dopamine system

Having obtained evidence that CSS leads to activation of microglia

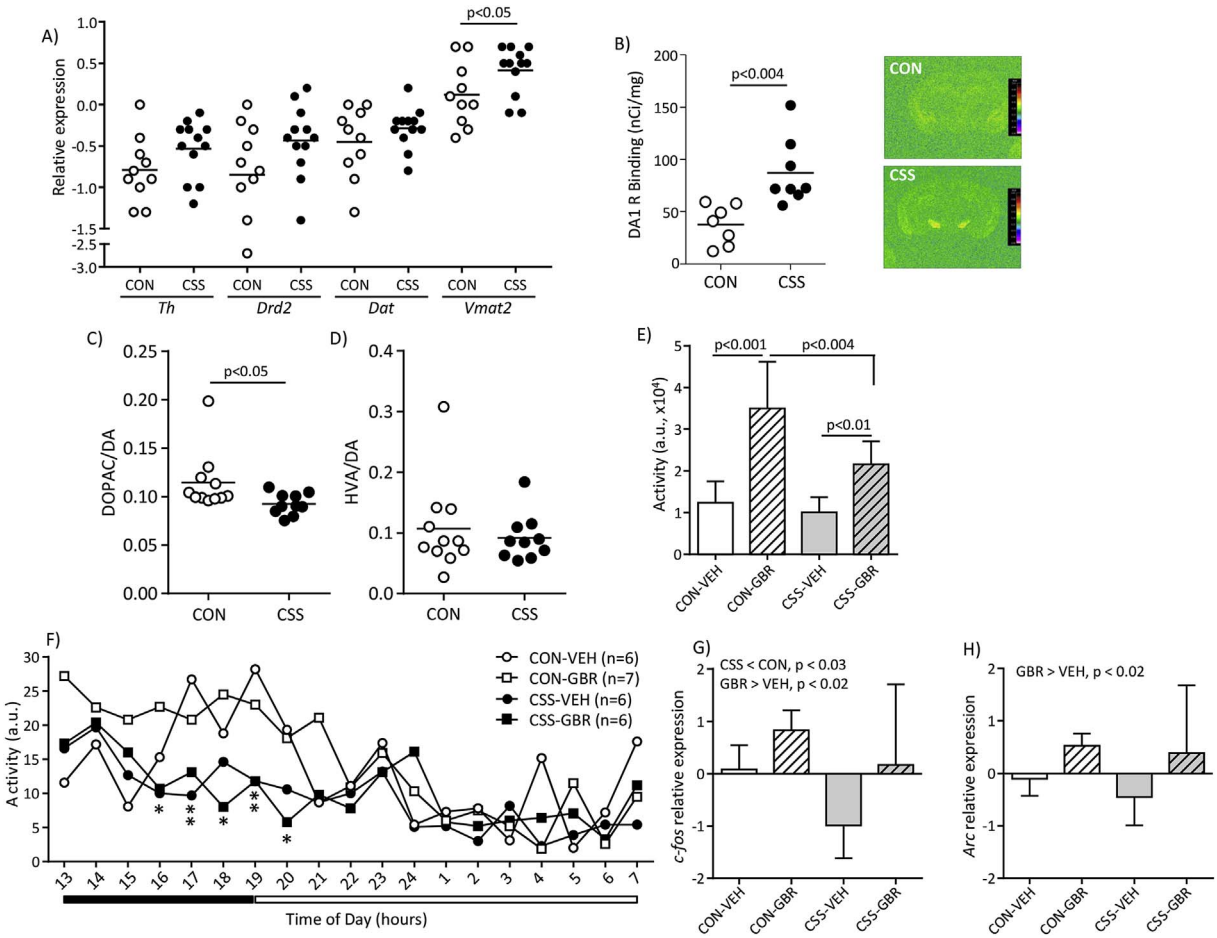

Fig. 5. Effects of CSS on the mesolimbic dopamine system (Expts 4, 6, 7 and 8). Expt 4: Fresh frozen brains were obtained from 12 CSS and 10 CON mice (same mice as in Fig. 3F). A) Comparison of VTA expression of genes encoding proteins for dopamine synthesis and signalling at day 16, as measured using qPCR: tyrosine hydroxylase (*Th*), dopamine receptor 2 (*Drd2*), dopamine transporter (*Dat*), vesicular monoamine transporter 2 (*Vmat2*). Expt 6: Fresh frozen brains were obtained from 8 CSS and 8 CON mice at day 16 for DA D1 and D2 receptor binding using autoradiography. B) VTA D1 receptor binding, and representative computer-enhanced autoradiograms of [^{3}H]SCH-23390 total binding in coronal sections including VTA from a CON and CSS mouse. The colour scale calibrates signal intensity against tritium standards. *p* value was obtained in an unpaired *t*-test. Expt 7: Fresh frozen brains were obtained from 10 CSS and 11 CON mice at day 16 for quantification of NAcc levels of dopamine (DA) and its metabolites DOPAC and HVA. B) NAcc DOPAC/DA ratio. C) NAcc HVA/DA ratio. *p* values were obtained in unpaired *t*-tests. Expt 8: Behavioural and NAcc immediate-early gene readouts for effects of CSS and DAT inhibitor GBR 12909 (6 mg/kg i.p.) at days 16–17. CSS and CON mice received either GBR 12909 or saline vehicle (VEH) on each of days 16 and 17. E) Day 16 total locomotor activity in an arena during 2 h, starting 30 min post-injection. Values are mean + SD. *p* values are for Stress X Drug ANOVA followed by *post hoc* Bonferonni tests. F) Day 16–17 home cage activity beginning 2.5 h post-injection and measured across the remaining active (dark) phase (i.e. 13.00–19.00 h) and subsequent inactive (light) phase (i.e. 19.00–7.00 h). Activity was sampled at 1 min intervals and average hourly values calculated. *p < 0.05, **p < 0.01 for Stress × Time interaction in repeated measures ANOVA followed by time-specific CSS vs. CON *post hoc* Bonferonni tests. G) Day 17 NAcc *c-fos* expression (mean ± SD) in fresh fixed brains collected 30 min after a second injection, measured using qPCR. H) Day 17 NAcc *Arc* expression (mean ± SD) measured under the same conditions as in F. *p* values were obtained in 2-way ANOVA followed by *post hoc* Bonferroni tests. (For interpretation of the references to colour in this figure legend, the reader is referred to the Web version of this article.)

and the kynurenine pathway in VTA and of the kynurenine pathway in NAcc, we investigated for CSS effects on the status and functioning of the VTA-NAcc DA system. In the same cohort in which CSS mice had higher VTA *Cd11b* expression, we measured VTA expression of several genes essential to DA synthesis or signalling, namely tyrosine hydroxylase (*Th*), vesicular monoamine transporter 2 (*Vmat2*), dopamine transporter (*Dat*) and dopamine receptor 2 (*Drd2*) (Fig. S1, Expt 4). In the case of *Vmat2*, VTA expression was higher in CSS mice ($t_{(20)} = -2.1$, $p < 0.05$) (Fig. 5A). For each of the other genes, whilst mean mRNA expression was higher in CSS than CON mice there was no significant effect of CSS: *Th* ($p = 0.14$), *Dat* ($p = 0.29$), *Drd2* ($p = 0.12$) (Fig. 5A). We then used autoradiography to determine D1 receptor binding in VTA and NAcc and D2 receptor binding in NAcc (Fig. S1, Expt 6). In VTA, D1 receptor binding was higher in CSS than in CON mice ($t(13) = 3.59$, $p < 0.004$, Fig. 5B). There was no effect of CSS on D1 receptor binding in NAcc (CON 232 ± 25 nCi/mg, CSS 242 ± 20, $p = 0.40$, data not shown), or on D2 receptor binding in NAcc (CON 22 ± 3 nCi/mg, CSS 22 ± 3, $p = 0.98$, data not shown). In the next experiment, HPLC-ED was used to investigate CSS effects on NAcc tissue levels of DA and its metabolites (Fig. S1, Expt 7). There was no significant effect of CSS on absolute levels of NAcc DA (CON 4.77 ± 1.15 ng/mg tissue, CSS 4.77 ± 1.33, $p = 0.99$), DOPAC (CON 0.53 ± 0.12, CSS 0.44 ± 0.14, $p = 0.15$) or HVA (CON 0.46 ± 0.21, CSS 0.42 ± 0.17, $p = 0.66$) (data not shown). However, the ratio DOPAC/DA, which provides the major measure of DA turnover, was reduced in the NAcc in CSS relative to CON mice ($t_{(19)} = 2.2$, $p < 0.05$, Fig. 5C). There was no CSS effect on the HVA/DA ratio ($p = 0.57$, Fig. 5D).

Building on the *ex vivo* evidence for reduced mesolimbic DA functioning in CSS mice, we investigated for *in vivo* and further *ex vivo* evidence using acute challenge with the dopamine transporter (DAT) inhibitor GBR 12909 (Fig. S1, Expt 8). On day 16, mice were injected i.p. with GBR 12909 or vehicle (VEH) and assessed in terms of effects on arena locomotor activity (Fig. 5E). In a 2 Stress (CON, CSS) x 2 Drug (VEH, GBR 12909) ANOVA, there were main effects of Stress ($F_{(1, 21)} = 7.4$, $p < 0.02$) and Drug ($F_{(1, 21)} = 34.7$, $p < 0.0005$) and a

trend to a Stress × Drug interaction effect ($F_{(1, 21)} = 3.7$, $p < 0.07$): in *post hoc* pairwise tests, activity was similar in CON-VEH and CSS-VEH mice, both CON-GBR mice ($p < 0.001$) and CSS-GBR mice ($p < 0.01$) were more active than their respective VEH groups, and CSS-GBR mice were less active than CON-GBR mice ($p < 0.004$). Thereafter, mice were returned to their home cage and activity was measured from 13:00 h to 07:00 h the following day. In a 2 Stress x 2 Drug x 19 Time-block (Hour) repeated measures ANOVA, there was a Stress × Time interaction ($F_{(18, 378)} = 1.9$, $p < 0.05$, Fig. 5F), with *post hoc* analysis identifying lower activity in CSS compared with CON mice across 16:00–20:00 h i.e. end of the active-dark phase (Fig. 5F). On day 17, mice received a second GBR 12909 or VEH challenge and were sacrificed after 30 min; brains were collected for qPCR analysis of the immediate-early genes *c-fos* and *Arc* in the NAcc. For *c-fos* expression there were main effects of Stress ($F_{(1, 21)} = 6.19$, $p < 0.03$) and Drug ($F_{(1, 21)} = 7.44$, $p < 0.02$) without interaction ($p = 0.57$) (Fig. 5G): *c-fos* expression was lower in CSS compared with CON mice, and higher in GBR 12909 compared with VEH mice, such that mean *c-fos* expression was lowest in CSS-VEH mice. For *Arc* expression, there was no Stress effect ($p = 0.40$) and a main effect of Drug ($F_{(1, 21)} = 6.06$, $p < 0.02$) with *Arc* expression higher in GBR 12909 compared with VEH mice (Fig. 5H). Therefore, the data suggest that GBR 12909 challenge revealed blunted DA functioning in CSS mice in terms of locomotor activity and NAcc *c-fos* expression.

3.3. CSS reduces operant behaviour for sucrose reward

In the final two experiments, CSS effects on behaviour directed at gustatory reward were investigated, firstly in terms of consumption of freely-available sweet-tasting reward in a two-bottle saccharin versus water test (Fig. S1, Expt 9). On day 16, there was no effect of CSS on the high absolute amount of saccharin drinking (CON 5.2 ± 2.1 g, CSS 5.3 ± 1.1 g, $p = 0.87$, data not shown); whilst all mice drank relatively little water, CSS mice drank more than CON mice (CON 0.08 ± 0.00 g, CSS 0.21 ± 0.02 g, $t_{(18)} = -2.35$, $p < 0.04$). Primarily due to the latter, CSS mice exhibited a lower saccharin preference at trend level (CON 98.1% ± 0.04%, CSS 96.1% ± 0.04%, $t_{(18)} = 1.96$, $p = 0.07$).

CSS effects on operant behaviour for sucrose-pellet reward were then investigated (Fig. S1, Expt 10). For operant training, mice were standard-diet restricted so that body weight (BW) was 90–95% of baseline. At the final training stage mice had a limited interval of 10 s to make an operant response at the feeder to initiate the trial and a limited interval of 6 s to make an operant response at the single operant stimulus to trigger pellet delivery back at the feeder. When all mice were trained, CSS/CON were carried out and sufficient standard diet was provided to maintain each mouse at 100% baseline BW: during these 15-days CON mice weighed 100 ± 3% baseline BW and CSS mice were mildly higher at 103 ± 3% baseline BW ($t_{(25)} = -3.08$, $p < 0.005$, data not shown); the absolute BW was similar in CON (26.5 ± 1.4 g) and CSS mice (26.9 ± 1.2 g) ($p = 0.38$). At CSS day 8, mice were studied in the fixed-ratio 1 (FR1) test with parameters the same as at the final training stage. To control for any effect of % baseline BW, it was included as covariate in ANCOVA for CSS effects. Operant responding for reward was reduced in CSS compared with CON mice in terms of: higher number of omissions to initiate trials ($F_{(1, 24)} = 5.70$, $p < 0.03$, Fig. 6A), fewer pellets earned ($F_{(1, 24)} = 5.29$, $p < 0.04$, Fig. 6C), and greater session duration ($F_{(1, 24)} = 7.55$, $p < 0.02$, Fig. 6D). CSS was without effect on omissions to emit a stimulus response in initiated trials ($p = 0.67$, Fig. 6B) and on latency to collect pellets (CON 1.46 ± 0.68 s, CSS 2.17 ± 1.43 s, $p = 0.13$). Inter-individual variability was greater in CSS than CON mice on some measures (Fig. 6A, C).

Beginning on day 16, these mice were investigated in the two stages of the learned non-reward (LNR) test. This comprised a spatial discrimination (SD) stage with one rewarded and one non-rewarded operant stimulus, followed by a LNR stage with the rewarded operant stimulus removed, the previously non-rewarded operant stimulus now the rewarded operant stimulus, and a novel non-rewarded operant stimulus (Fig. S2). For SD and LNR stages, each daily test consisted of 70 trials divided into 10-trial blocks, the criterion for learning was nine correct responses within any one block, the same stage was repeated the next day if criterion was not attained, and for each measure the total number (cumulative across test days) of occurrences until attaining criterion was used for analysis. Mice were maintained at 95% baseline BW across the testing period: actual BW was 97 ± 4% baseline in CON mice and 95 ± 2% baseline in CSS mice ($p = 0.23$, data not shown). At the SD stage, mice required 1–5 daily tests to attain the learning criterion (CON 1–4, CSS 1–5). There was no effect of CSS on any measure: omissions to initiate trials (CON 24 ± 25, CSS 33 ± 39, $p = 0.53$), omissions to emit choice responses in initiated trials (CON 17 ± 12, CSS 27 ± 28, $p = 0.25$), incorrect choice responses (CON 24 ± 19, CSS 19 ± 22, $p = 0.52$), total errors (CON 65 ± 52, CSS 79 ± 79, $p = 0.62$), and correct choice responses (CON 46 ± 22, CSS 62 ± 34, $p = 0.18$) (data not shown). At the LNR stage, mice required 1–8 daily tests to attain the learning criterion (CON 1–4, CSS 1–8). Relative to CON mice, CSS mice exhibited deficits in reward-directed behaviour in terms of: higher number of omissions to initiate trials ($t_{(14)} = -2.4$, $p < 0.04$, Fig. 6E), higher incorrect choice responses in initiated trials i.e. avoiding the previously non-rewarded operant stimulus ($t(24) = -2.2$, $p < 0.04$, Fig. 6G), and higher total errors ($t(18) = -2.4$, $p < 0.05$, Fig. 6H). CSS and CON mice behaved similarly in terms of omissions to emit choice responses in initiated trials ($p = 0.16$, Fig. 6F) and correct choice responses (CON 57 ± 22, CSS 43 ± 27, $p = 0.19$). Inter-individual variability was greater in CSS than CON mice on most LNR measures.

4. Discussion

The present mouse study demonstrates that chronic social stress leads to a constellation of: immune-inflammation activation in the periphery, immune activation in the VTA-NAcc DA pathway, reduced VTA-NAcc DA pathway functioning, and reduced NAcc DA-dependent reward-directed behaviour. To our knowledge this is the first demonstration of the co-occurrence of each of these altered system states within one stress model. Evidence of co-occurrence is of course not evidence of causality. However, the overall finding that these altered states do co-occur following stress is both an essential pre-requisite and provides major justification for proposing a causal pathway linking them (e.g. (Felger and Treadway, 2017)). Fig. 7 illustrates the current findings with respect to each of the stress-induced system states; it also presents these system states within the hypothesized causal pathway, from stress activation of the immune system to altered mesolimbic DA function and resultant impaired reward processing. Here we discuss the findings within each of the stress-induced states in terms of how these expand on and complement existing knowledge, and also present some specific hypotheses linking adjacent states in the pathway. This mouse model can now be utilised to investigate cause-effect pathophysiological mechanisms at the interfaces between immunity, dopamine reward circuitry and behaviour, with the major aim of identifying molecular targets for treatment of stress-related reward psychopathologies.

Building on previous evidence that CSS mice exhibit splenomegaly (Azzinnari et al., 2014; Fuertig et al., 2016) this study demonstrates that CSS leads to increased myeloid splenocytes, including granulocytes and inflammatory monocytes. Mouse repeated social defeat also increases splenic granulocytes and monocytes (Avitsur et al., 2002). The splenic myeloid cells of CSS mice had higher expression of the proinflammatory cytokines TNF-α and IFN-γ, suggesting that they contribute to the increased blood levels of these cytokines reported for CSS mice (Azzinnari et al., 2014; Fuertig et al., 2016). Splenic myeloid cell surface MHC II expression was reduced in CSS mice; higher levels of intracellular MHC II promote an innate immune response (Liu et al., 2011) and it will be important to determine whether CSS leads to

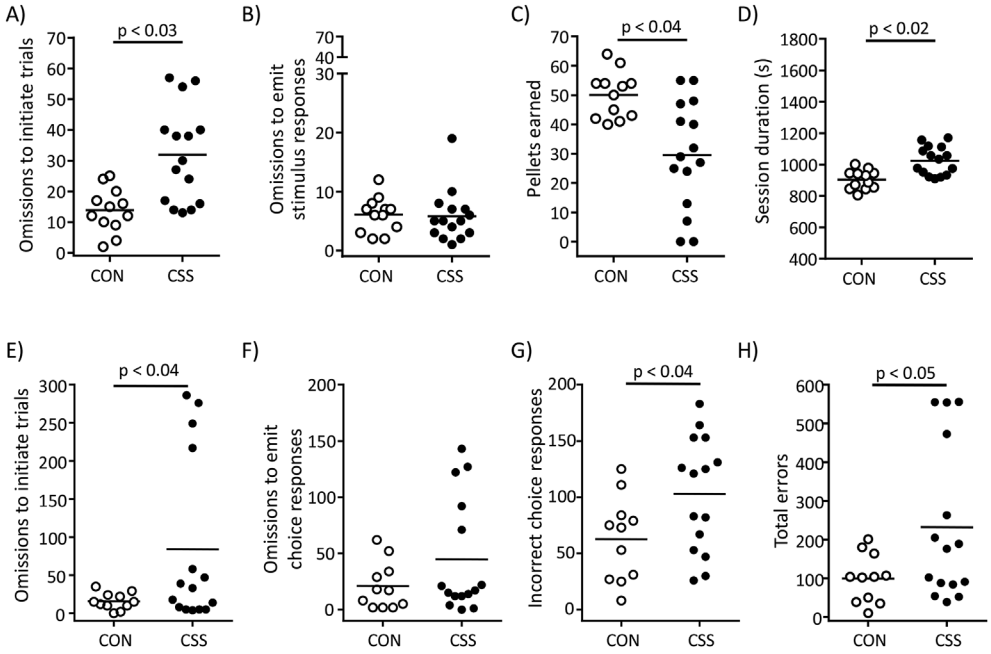

Fig. 6. Effects of CSS on reward-directed behaviour in operant tests (Expt 10). At CSS day 8, 15 CSS and 12 CON mice were tested in a fixed ratio 1 schedule (FR1) test with a time limit of 10 s to initiate each trial and 6 s to emit an operant response at a single stimulus. A) Omissions to initiate trials. B) Omissions to emit stimulus response in initiated trials. C) Pellets earned. D) Session duration. *p* values were obtained in ANCOVA with % baseline body weight included as covariate. Beginning at day 16, CSS and CON mice were tested in the learned non-reward (LNR) test that comprised a time limit of 10 s to initiate each trial and 6 s to emit an operant choice response. At the simple discrimination stage there was no significant effect of CSS. At the LNR stage the rewarded operant stimulus was removed, the previously non-rewarded operant stimulus was now the rewarded operant stimulus, and a novel non-rewarded operant stimulus was introduced (see Fig. S2): E) Omissions to initiate trials. F) Omissions to emit choice response on initiated trials. G) Incorrect choice responses. H) Total errors. *p* values were obtained in unpaired *t*-tests. One CON mouse was a statistical outlier and was removed from the dataset.

intracellular accumulation of MHC II. Regarding effects on the adaptive immune system, splenic total lymphocytes were reduced in CSS compared with CON mice. This reduction was not attributable to splenic $CD4^+$ or $CD8^+$ T cells and might reflect less B cells; future experiments will need to test for this. Despite the overall decrease in lymphocytes and lack of effect on total $CD4^+$ T cells, CSS mice had more splenic T helper 17 cells than did CON mice. Th17 cells secrete proinflammatory cytokines, including IL-17A, IL-17F, IL-22, IL-6 and TNF-α (Kimura and Kishimoto, 2010). Numerical imbalance between Th17 and Treg cells occurs in mice exposed to chronic or acute stress (Beurel et al., 2013; Hong et al., 2012), and chronic social stress leads to increased T-cell effector functions in the periphery (Schmidt et al., 2010). Peripheral or CNS infusion of Th17 cells leads to depression-relevant behaviour in mice, although reward-directed behaviours were not studied (Beurel

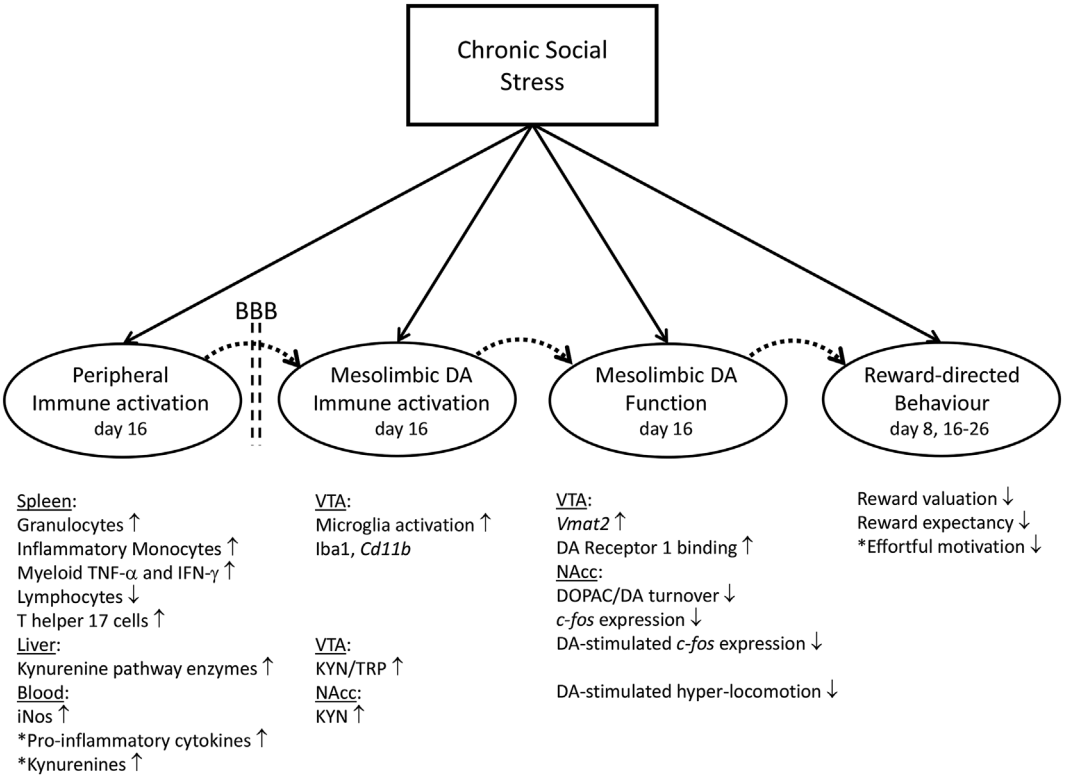

Fig. 7. Diagram depicting each of the system states that was impacted by 15-day chronic social stress and a hypothesized causal pathway, from stress activation of the immune system to altered mesolimbic DA function and resultant impaired reward processing. The solid arrows linking chronic social stress with each separate system depict the causal relationships identified in this study. The dashed arrow linking each pair of systems depicts the causal relationship hypothesized to exist between them which can be investigated in the present model. For each system state the factors that were studied and demonstrated to be affected by CSS are indicated, with either a quantitative increase (↑) or decrease (↓) in the factor in CSS compared with CON mice. BBB = blood-brain barrier and denotes that peripheral-to-brain immune activation would require BBB passage in the case of some mediating pathways. CSS effects on factors marked with an asterisk were not analysed in this study and the effects were demonstrated in previous studies.

et al., 2013). Th17 cells are important in autoimmune diseases (Aranami and Yamamura, 2008), including multiple sclerosis which is highly comorbid with depression (Slyepchenko et al., 2016). It has been proposed that depression is caused by stress-induced Th17 cell-mediated autoimmunity in some patients (Chen et al., 2011; Slyepchenko et al., 2016). Whilst it activated splenic myeloid cells, in the same mice CSS was without effect on whole-brain microglia, macrophages or lymphocytes. Previous mouse studies have demonstrated that stress induces a generalized activation of microglia (Gerecke et al., 2013; Nair and Bonneau, 2006; Wohleb et al., 2012), and indeed monocyte trafficking to the brain (Wohleb et al., 2014). One possible explanation for the current absence of CSS effects on whole-brain microglia/macrophage levels is that stress-induced activation occurs in a specific time window (Kreisel et al., 2014; Nair and Bonneau, 2006). We then investigated CSS effects on microglia activation in the regions of interest: Iba1 immunoreactivity was increased in VTA and not in NAcc, and increased expression of the macrophage/microglia gene *Cd11b* in VTA corroborated this finding. We also measured Iba1 immunoreactivity in the stress-sensitive regions of the amygdala and prefrontal cortex and there was no increase in CSS mice (data not shown). Activation of Iba1 in the VTA and other regions, e.g. medial prefrontal cortex, has been reported for mice exposed to 10-day chronic social defeat (Tanaka et al., 2012). Future studies will need to investigate the time course of CSS effects on microglia activation as well as brain monocytes and T cells, and also whether the present evidence that VTA is more susceptible than NAcc to CSS-induced microglia activation can be substantiated. The latter will also need to investigate CSS effects on Iba1-based microglia morphology including cell body to cell size ratio (Hovens et al., 2014).

A further important stress-responsive peripheral-to-CNS immune pathway is tryptophan-kynurenine (KYN) catabolism: Increases in TNF-α, IFN-γ and IL-6 activate indoleamine 2,3-dioxygenase (IDO1) and tryptophan 2,3-dioxygenase (TDO2) expression in immune and other cells, promoting tryptophan-KYN catabolism in periphery and brain (Campbell et al., 2014; Haroon et al., 2016; Schwarcz et al., 2012). Peripheral activation of the kynurenine pathway occurs in depression and other stress-related psychiatric disorders (Haroon et al., 2012; Kim et al., 2012; Savitz et al., 2015a, 2015b; Steiner et al., 2011; Sublette et al., 2011). We reported that CSS leads to increased blood levels of KYN, 3-HK and kynurenic acid, and to increased KYN and 3-HK levels in amygdala, hippocampus and prefrontal cortex (Fuertig et al., 2016). Chronic mild stress in mice induced activation of KYN-pathway enzymes in skeletal muscle and liver and increases in plasma KYN and brain 3-HK (Agudelo et al., 2014). Here, CSS led to increased liver expression of genes encoding KYN-pathway enzymes, namely *Tdo1*, *Ido2*, *Tdo2*, *Kynu* and *3-Haao* (*Ido1* has negligible expression in liver (Dai and Zhu, 2010; Fuertig et al., 2016)). Future study will need to determine whether the stimulatory effect of CSD on liver kynurenine pathway enzyme transcription also leads to increased expression of the respective enzymes per se. In VTA, CSS mice had a higher KYN/TRP ratio, and in NAcc they had higher absolute KYN levels, whilst 3-HK was unaffected in these regions of interest. Given that microglia were activated in VTA of CSS mice, both peripheral and local synthesis could contribute to the increase in KYN-pathway activity in this region (Fuertig et al., 2016; Schwarcz et al., 2012). Inducible nitric oxide synthase (iNOS), the synthase responsible for catalysing the production of nitric oxide in the context of immune regulation, was higher in the plasma of CSS mice; these were the same mice in which liver expression of KYN-pathway enzymes was up-regulated. Synthesis of iNOS is activated by both pro-inflammatory cytokines (Sheng et al., 2011) and kynurenines (Colin-Gonzalez et al., 2013), peripheral levels of both of which are increased by CSS (Azzinnari et al., 2014; Fuertig et al., 2016). Nitric oxide and kynurenines promote oxidative stress as accumulation of reactive oxygen species (ROS), to regulate immune responses (Wink et al., 2011). However, in the VTA, high ROS levels contribute to oxidation and deactivation of the enzyme cofactor for DA synthesis, tetrahydrobiopterin (Bove et al., 2005; Felger and Miller, 2012; Felger and Treadway, 2017). Future studies with the CSS model will investigate causal involvement of oxidative stress in CSS-induced VTA-NAcc DA pathway changes.

The current assessment of CSS effects on the VTA-NAcc DA pathway included VTA expression of certain genes encoding DA synthesis and transport proteins. Expression of the genes encoding tyrosine hydroxylase, the DA transporter and DA receptor 2 was not affected consistently by CSS. CSS did lead to increased VTA gene expression of vesicular monoamine transporter 2 (*Vmat2*). Given that CSS led to immune activation in VTA, increased *Vmat2* expression might reflect compensatory up-regulation of DA axonal transport. Furthermore, CSS mice exhibited increased VTA D1 receptor binding. In the VTA, D1 receptors are expressed at the terminals of axons of glutamate neurons (e.g. prefrontal cortex), GABA neurons (e.g. NAcc, ventral pallidum) and VTA GABA interneurons, where they bind DA to regulate local release of glutamate and GABA at synapses with VTA DA neurons (Lu et al., 1997). Stimulation of VTA D1 receptors facilitates release of glutamate that excites DA neurons (Rahman and McBride, 2000), but also facilitates release of GABA that inhibits DA neurons (Klitenick et al., 1992). Local VTA microinjection of D1 receptor antagonist inhibits reward sensitivity (Galaj et al., 2014). Therefore, depending on which VTA neurons acquire the increased D1 receptor binding in CSS mice, the CSS-induced increase in VTA D1 receptor binding could constitute a neuroplastic compensation for attenuated DA release in terminal areas. The VTA DA neurons project to NAcc (core and shell), prefrontal cortex, amygdala and hippocampus. In NAcc, whilst there was no CSS effect on absolute tissue levels of DA and its metabolites DOPAC and HVA, CSS mice had lower NAcc DA turnover in terms of a lower DOPAC/DA ratio. A previous mouse study reported a higher DOPAC/DA ratio in NAcc and mPFC after a single social defeat and a lower ratio after 10-day chronic social defeat (Tanaka et al., 2012). Reduced DA turnover in the basal ganglia has been reported for depression (Bowden et al., 1997). There was no CSS effect on D1 or D2 receptor binding in NAcc.

We further investigated CSS effects on DA function using acute challenge with the selective DA transporter blocker/reuptake inhibitor GBR 12909. In mice, GBR 12909 increases extracellular DA levels in NAcc and dorsal striatum (Abdallah et al., 2009), induces hyper-locomotion (Irifune et al., 1995) and up-regulates NAcc expression of immediate-early genes *c-fos* and *Arc* (Iadarola et al., 1993). NAcc DA depletion reduces responsiveness to psychostimulants (Koob et al., 1978). Whilst CSS and CON mice did not differ in basal locomotor activity in an arena, GBR 12909 challenge resulted in attenuated hyper-locomotion in CSS compared with CON mice. GBR 12909 hypo-sensitivity of CSS mice could be due to higher DA transporter function; however, there was no CSS effect on VTA *Dat* expression. Another possibility is down-regulation of post-synaptic DA signalling in striatal neurons. Whilst there was no CSS effect on NAcc D1 or D2 receptor binding, NAcc expression of the immediate early gene *c-fos* (although not *Arc*) was down-regulated in CSS mice, both in basal state and following GBR 12909. These *c-fos* findings are in line with previous studies demonstrating that stress attenuates the acute increase in CNS *c-fos* expression induced by novel stimulus exposure (Ons et al., 2010; Ostrander et al., 2006; Stone et al., 2007). Future studies will investigate CSS effects on NAcc expression of genes and proteins involved in DA post-synaptic signalling; down-regulated expression of genes important in post-synaptic DA signalling has already been demonstrated for amygdala of CSS mice (Azzinnari et al., 2014).

To investigate CSS effects on reward-directed behaviour we used tests of reward consumption and, in particular, effortful and discriminatory operant behaviour. In a previous study, CSS led to reduced operant responding for sucrose pellets on a progressive ratio schedule indicating attenuated effortful motivation, and to reduced responding at the correct stimulus in a reversal learning test indicating attenuated reward expectancy (Bergamini et al., 2016a). In the two-bottle test,

several studies report decreased preference for sweet solution relative to water in chronic social defeat mice (Covington et al., 2009; Henriques-Alves and Queiroz, 2015; Krishnan et al., 2007). The reduced saccharin preference observed in CSS mice was at trend level and due to increased water consumption, with the latter probably due to their increased feeding (Bergamini et al., 2016a). Interestingly, in depressed patients, reduced consummatory pleasure as measured by the Sweet taste test is not reduced relative to controls (Dichter et al., 2010; Treadway, 2016; Treadway and Zald, 2011). The FR1 test was conducted at CSS day 8: already at this time-point reward-directed behaviour was reduced in CSS mice, with the major deficit being increased number of omissions to initiate trials within the limited time interval. This could reflect attenuated reward valuation and/or psychomotor slowing in CSS mice; the absence of a CSS effect on reward-collect latency makes the former more likely. In the learned non-reward (LNR) test, CSS was without effect at the simple discrimination stage, indicating that reward valuation was intact under moderate food deprivation. At the subsequent LNR stage, CSS mice made more omissions to initiate trials and more incorrect-choice responses. The increase in incorrect choice responding indicates that CSS mice have attenuated: reward expectancy which impairs their learning of the new contingency between stimulus and reward, and/or reward valuation which reduces their responding to the previously non-rewarded and now rewarded stimulus. In a set-shifting operant task used to assess the learned non-reward effect in humans, depressed patients also exhibited reduced responding to previously non-rewarded and now rewarded stimuli compared with healthy controls (Michopoulos et al., 2006). Dopamine signalling modulates reward valuation and expectancy in rodents (Berridge and Kringelbach, 2013). CSS actually recapitulated the effects of NAcc DA depletion with 6-hydroxydopamine, which also led to more omissions to initiate trials and incorrect-choice responses specific to the LNR stage (Bergamini et al., 2016b). Depressed patients exhibit lower anticipatory reward valuation (Sherdell et al., 2012), including under effortful conditions (Hershenberg et al., 2016; Treadway et al., 2012; Yang et al., 2014), and this is associated with reduced activity in the ventral striatum (Arrondo et al., 2015). In rodents, acute inflammatory challenge (e.g. IL-1β, LPS, CD40 agonist antibody) induces sickness followed by a period of reduced consumption of and preference for sweet reward under freely available conditions (Biesmans et al., 2013; Cathomas et al., 2015). In addition, similarly to CSS mice and depressed humans, inflammation leads to reduced anticipatory reward valuation and particularly under effortful conditions (Cathomas et al., 2015; Nunes et al., 2014; Vichaya et al., 2014). Some CSS mice exhibited similar scores to CON mice in the behavioural tests. We consider this to be primarily due to CSS-induced changes in appetite regulators, e.g. lower plasma leptin levels (Bergamini et al., 2016a), that were only partially compensated by feeding more standard diet to CSS than CON mice. Such changes would counteract the impact of CSS attenuation of VTA-NAcc-DA pathway function in some mice. Tests that measure effortful responding for sucrose when standard diet is freely available in the operant chamber (Salamone et al., 2016; Vichaya et al., 2014) will probably identify more consistent effects of CSS on reward-directed behaviour.

Using the manipulation of 10-day chronic social defeat (CSD) some laboratories divide mice into susceptible versus resilient sub-groups based on subsequent passive avoidance or active approach, respectively, of the aggressor mouse strain (Krishnan et al., 2007). It has been reported that a high plasma level of interleukin 6 (IL-6) after 1 day of stress defeat provides a biomarker for subsequent susceptibility, plasma IL-6 level remains chronically elevated after CSD (Hodes et al., 2014), and IL-6 passage from blood to brain contributes to loss of sucrose preference and reduced mobility in the forced swim test in CSD-susceptible mice (Menard et al., 2017). It has not been reported whether susceptible and resilient mice differ in their behaviour during the daily 10-min attack sessions. In rat, using a 5-day repeated resident-intruder paradigm resulted in individuals with short versus long latency to assume a defeat body posture, and the former group had higher levels of post-stress brain IL-1β mRNA and reduced sucrose preference (Wood et al., 2015). In line with our previous studies with 15-day CSS, in the present study we have used an inclusive experimental design in terms of not separating CSS mice into susceptible versus resilient sub-groups. With this design and sample sizes of 10–12 CSS versus CON mice we have demonstrated robust and reproducible effects of CSS on depression-relevant behaviour, brain functional connectivity and metabolism, and blood immune-inflammatory markers ((Azzinnari et al., 2014; Bergamini et al., 2016a; Fuertig et al., 2016; Grandjean et al., 2016); present study). We observe each CSS attack: as described in our original report on this manipulation, any back-fighting by BL/6 mice with aggressor CD-1 mice is restricted to days 1–5 and thereafter all mice exhibit a defeat/submissive body posture and emit submissive vocalizations during each attack session (Azzinnari et al., 2014). Plasma levels of each of TNF-α, INF-γ and IL-6 are increased on day 16 in CSD mice (Azzinnari et al., 2014; Fuertig et al., 2016). In future studies it will be interesting to investigate whether the latency to exhibit submissive behaviour and/or basal plasma cytokine levels predict the extent of post-CSD effects within the CSD group, in addition to the overall CSD effects relative to CON mice.

In summary, this mouse study provides comprehensive evidence that chronic social stress leads to a constellation of immune-inflammation activation in the periphery, immune activation in the VTA-NAcc DA pathway, reduced VTA-NAcc DA pathway functioning, and reduced NAcc DA-dependent reward-directed behaviour. This model can now be applied to test causal hypotheses on pathophysiological mechanisms via which immune activation impacts on dopamine functioning in the mesolimbic pathway, with the aim of identifying targets for treatment of stress-related psychopathologies of reward processing.

Acknowledgments

We are grateful to Björn Henz and Alex Osei for animal care and Zia-Uddin Ahmed for technical assistance. This research was funded by the Swiss National Science Foundation (grant 31003A_160147 to CRP) and research collaboration between Boehringer Ingelheim Pharma GmbH & Co. KG, Germany and PLaTRAD, University of Zurich, Switzerland. TS was funded by the Clinical Research Priority Program (CRPP) Multiple Sclerosis of the University of Zurich.

Appendix A. Supplementary data

Supplementary data related to this article can be found at http://dx.doi.org/10.1016/j.ynstr.2018.01.004.

References

Abdallah, L., Bonasera, S.J., Hopf, F.W., O'Dell, L., Giorgetti, M., Jongsma, M., Carra, S., Pierucci, M., Di Giovanni, G., Esposito, E., Parsons, L.H., Bonci, A., Tecott, L.H., 2009. Impact of serotonin 2C receptor null mutation on physiology and behavior associated with nigrostriatal dopamine pathway function. J. Neurosci. 29, 8156–8165.

Agudelo, L.Z., Femenia, T., Orhan, F., Porsmyr-Palmertz, M., Goiny, M., Martinez-Redondo, V., Correla, J.C., Izadi, M., Bhat, M., Schuppe-Koistinen, I., Pettersson, A.T., Ferreira, D.M.S., Krook, A., Barres, R., Zierath, J.R., Erhardt, S., Lindskog, M., Ruas, J.L., 2014. Skeletal muscle PGC-1A1 modulates kynurenine metabolism and mediates resilience to stress-induced depression. Cell 159, 33–45.

Aranami, T., Yamamura, T., 2008. Th17 Cells and autoimmune encephalomyelitis (EAE/MS). Allergol. Int. 57, 115–120.

Arrondo, G., Segarra, N., Metastasio, A., Ziaudden, H., Spencer, J., Reinders, N.R., Dudas, R.B., Robbins, T.W., Fletcher, P.C., Murray, G.K., 2015. Reduction in ventral striatal activity when anticipating a reward in depression and schizophrenia: a replicated cross-diagnostic finding. Front. Psychol. 6 128010.3389/fpsyg.2015.01280.

Avitsur, R., Stark, J.L., Dhabhar, F.S., Sheridan, J.F., 2002. Social stress alters splenocyte phenotype and function. J. Neuroimmunol. 132, 66–71.

Azzinnari, D., Sigrist, H., Staehli, S., Palme, R., Hildebrandt, T., Leparc, G., Hengerer, B., Seifritz, E., Pryce, C.R., 2014. Mouse social stress induces increased fear conditioning, helplessness and fatigue to physical challenge together with markers of altered immune and dopamine function. Neuropharmacology 85, 328–341.

Bergamini, G., Cathomas, F., Auer, S., Sigrist, H., Seifritz, E., Patterson, M., Gabriel, C., Pryce, C.R., 2016a. Mouse psychosocial stress reduces motivation and cognitive

function in operant reward tests: a model for reward pathology with effects of agomelatine. Eur. Neuropsychopharmacol 26, 1448–1464.
Bergamini, G., Sigrist, H., Ferger, B., Singewald, N., Seifritz, E., Pryce, C.R., 2016b. Depletion of nucleus accumbens dopamine leads to impaired reward and aversion processing in mice: relevance to motivation pathologies. Neuropharmacology 109, 306–319.
Berridge, K.C., Kringelbach, M.L., 2013. Neuroscience of affect: brain mechanisms of pleasure and displeasure. Curr. Opin. Neurobiol. 23, 294–303.
Beurel, E., Harrington, L.E., Jope, R.S., 2013. Inflammatory T helper 17 cells promote depression-like behavior in mice. Biol. Psychiatr. 73, 622–630.
Bierhaus, A., Wolf, J., Andrassy, M., Rohleder, N., Humpert, P.M., Petrov, D., Ferstl, R., von Eynatten, M., Wendt, T., Rudofsky, G., Joswig, M., Morcos, M., Schwaninger, M., McEwen, B., Kirschbaum, C., Nawroth, P.P., 2003. A mechanism converting psychosocial stress into mononuclear cell activation. PNAS 100, 1920–1925.
Biesmans, S., Meert, T.F., Bouwknecht, J.A., Acton, P.D., Davoodi, N., De Haes, P., Kuijlaars, J., Langlois, X., Matthews, L.J.R., Ver Donck, L., Hellings, N., Nuydens, R., 2013. Systemic immune activation leads to neuroinflammation and sickness behavior in mice. Mediators Inflamm 1–14 ID 271359.
Bove, J., Prou, D., Perier, C., Przedborski, S., 2005. Toxin-induced models of Parkinson's disease. NeuroRx 2, 484–494.
Bowden, C., Cheetham, S.C., Lowther, S., Katona, C.L., Crompton, M.R., Horton, R.W., 1997. Reduced dopamine turnover in the basal ganglia of depressed suicides. Brain Res. 769, 135–140.
Campbell, B.M., Charych, E., Lee, A.W., Möller, T., 2014. Kynurenines in CNS disease: regulation by inflammatory cytokines. Front. Neurosci. 8, 1–22.
Capuron, L., Pagnoni, G., Drake, D.F., Woolwine, B.J., Spivey, J.R., Crowe, R.J., Votaw, J.R., Goodman, M.M., Miller, A.H., 2012. Dopaminergic mechanisms of reduced basal ganglia responses to hedonic reward during interferon alfa administration. Arch. Gen. Psychiatr. 69, 1044–1053.
Cathomas, F., Fuertig, R., Sigrist, H., Newman, G., Hoop, V., Bizzozzero, M., Mueller, A., Ceci, A., Hengerer, B., Seifritz, E., Fontana, A., Pryce, C.R., 2015. CD40-induced inflammation in mice leads to sustained emotional and cognitive dysfunctions coincident with altered tryptophan metabolsim: a model for depression-autoimmune disease comorbidity. Brain Behav. Immun. 50, 125–140.
Chen, Y., Jiang, T., Chen, P., Ouyang, J., Xu, G., Zeng, Z., Sun, Y., 2011. Emerging tendency towards autoimmune process in major depressive patients: a novel insight from TH17 cells. Psychiatr. Res. 188, 224–230.
Chiang, J.J., Eisenberger, N.I., Seeman, T.E., Taylor, S.E., 2012. Negative and competitive social interactions are related to heightened proinflammatory cytokine activity. Proc. Natl. Acad. Sci. U. S. A 109, 1878–1882.
Colin-Gonzalez, A.L., Maldonado, P.D., Santamaria, A., 2013. 3-Hydroxykynurenine: an intriguing molecule exerting dual actions in the central nervous system. Neurotoxicology 34, 189–204.
Covington, H.E., Maze, I., LaPlant, Q.C., Vialou, V.F., Ohnishi, Y.N., Berton, O., Fass, D.M., Renthal, W., Rush, A.J., Wu, E.Y., Ghose, S., Krishnan, V., Russo, S.J., Tamminga, C.A., Haggarty, S.J., Nestler, E.J., 2009. Antidepressant effects of histone deacetylase inhibitors. J. Neurosci. 29, 11451–11460.
Cuthbert, B.N., Insel, T.R., 2013. Toward the future of psychiatric diagnosis: the seven pillars of RDoC. BMC Med. 11, 126.
Dai, X., Zhu, B.T., 2010. Indoleamine 2,3-dioxygenase tissue distribution and cellular localization in mice: implications for its biological functions. J. Histochem. Cytochem. 58, 17–28.
Dalton, V.S., Zavitsanou, K., 2011. Rapid changes in d1 and d2 dopamine receptor binding in striatal subregions after a single dose of phencyclidine. Clin Psychopharmacol Neurosci 9, 67–72.
Dantzer, R., Walker, A.K., 2014. Is there a role for glutamate-mediated excitotoxicity in inflammation-induced depression? J Neural Transm (Vienna) 121, 925–932.
Dichter, G.S., Smoski, M.J., Kampov-Polevoy, A.B., Gallop, R., Garbutt, J.C., 2010. Unipolar depression does not moderate responses to the sweet taste test. Depress. Anxiety 27, 859–863.
Dowlati, Y., Herrmann, N., Swardfager, W., Liu, H., Sham, L., Reim, E.K., Lanctot, K.L., 2010. A meta-analysis of cytokines in major depression. Biol. Psychiatr. 67, 446–457.
DSM-5, 2013. Diagnostic and Statistical Manual of Mental Disorders, fifth ed. Revision American Psychiatric Association, Washington, DC (American Psychiatric Association, Washington, DC).
Dunlop, B.W., Nemeroff, C.B., 2007. The role of dopamine in the pathophysiology of depression. Arch. Gen. Psychiatr. 64, 327–337.
Eisenberger, N.I., Berkman, E.T., Inagaki, T.K., Rameson, L.T., Mashal, N.M., Irwin, M.R., 2010. Inflammation-induced anhedonia: endotoxin reduces ventral striatum responses to reward. Biol. Psychiatr. 68, 748–754.
Felger, J.C., Li, Z., Haroon, E., Woolwine, B.J., Jung, M.Y., Hu, X., Miller, A.H., 2016. Inflammation is associated with decreased functional connectivity within corticostriatal reward circuitry in depression. Mol. Psychiatr. 21, 1358–1365.
Felger, J.C., Miller, A.H., 2012. Cytokine effects on the basal ganglia and dopamine function: the subcortical source of inflammatory malaise. Front. Neuroendocrinol. 33, 315–327.
Felger, J.C., Mun, J., Kimmel, H.L., Nye, J.A., Drake, D.F., Hernandez, C.R., Freeman, A.A., Rye, D.B., Goodman, M.M., Howell, L.L., Miller, A.H., 2013. Chronic interferon-alpha decreases dopamine 2 receptor binding and striatal dopamine release in association with anhedonia-like behavior in nonhuman primates. Neuropsychopharmacology 38, 2179–2187.
Felger, J.C., Treadway, M.T., 2017. Inflammation effects on motivation and motor activity: role of dopamine. Neuropsychopharmacology 42, 216–241.
Ferretti, M.T., Merlini, M., Spani, C., Gericke, C., Schweizer, N., Enzmann, G., Engelhardt, B., Kulic, L., Suter, T., Nitsch, R.M., 2016. T-cell brain infiltration and immature antigen-presenting cells in transgenic models of Alzheimer's disease-like cerebral amyloidosis. Brain Behav. Immun. 54, 211–225.
Franklin, K.B.J., Paxinos, G., 2008. The Mouse Brain: in Stereotaxic Coordinates, Compact, third ed. Elsevier, Amsterdam.
Fuertig, R., Azzinnari, D., Bergamini, G., Cathomas, F., Sigrist, H., Seifritz, E., Vavassori, S., Luippold, A., Hengerer, B., Ceci, A., Pryce, C.R., 2016. Mouse chronic social stress increases blood and brain kynurenine pathway activity and fear behaviour: both effects are reversed by inhibition of indoleamine 2 3-dioxygenase. Brain Behav. Immun. 54, 59–72.
Galaj, E., Manuszak, M., Arastehmanesh, D., Ranaldi, R., 2014. Microinjections of a dopamine D1 receptor antagonist into the ventral tegmental area block the expression of cocaine conditioned place preference in rats. Behav. Brain Res. 272, 279–285.
Gerecke, K.M., Kolobova, A., Allen, S., Fawer, J.L., 2013. Exercise protects against chronic restraint stress-induced oxidative stress in the cortex and hippocampus. Brain Res. 1509, 66–78.
Golden, S.A., Covington, H.E., Berton, O., Russo, S.J., 2011. A standardized protocol for repeated social defeat stress in mice. Nat. Protoc. 6, 1183–1191.
Goldsmith, D.R., Haroon, E., Woolwine, B.J., Jung, M.Y., Wommack, E.C., Harvey, P.D., Treadway, M.T., Felger, J.C., Miller, A.H., 2016. Inflammatory markers are associated with decreased psychomotor speed in patients with major depressive disorder. Brain Behav. Immun. 56, 281–288.
Grandjean, J., Azzinnari, D., Seuwen, A., Sigrist, H., Seifritz, E., Pryce, C.R., Rudin, M., 2016. Chronic psychosocial stress in mice leads to changes in brain functional connectivity and metabolite levels comparable to mouse brain. Neuroimage 142, 544–552.
Gruenewald, T.L., Cohen, S., Matthews, K.A., Tracy, R., Seeman, T.E., 2009. Association of socioeconomic status with inflammation markers in black and white men and women in the Coronary Artery Risk Development in Young Adults (CARDIA) study. Soc. Sci. Med. 69, 451–459.
Haroon, E., Fleischer, C.C., Felger, J.C., Chen, X., Woolwine, B.J., Patel, T., Hu, X.P., Miller, A.H., 2016. Conceptual convergence: increased inflammation is associated with increased basal ganglia glutamate in patients with major depression. Mol. Psychiatr. 21, 1351–1357.
Haroon, E., Raison, C.L., Miller, A.H., 2012. Psychoneuroimmunology meets neuropsychopharmacology: translational implications of the impact of inflammation on behavior. Neuropsychopharmacology 37, 137–162.
Harrison, N.A., Voon, V., Cercignani, M., Cooper, E.A., Pessiglione, M., Critchley, H.D., 2016. A neurocomputational account of how inflammation enhances sensitivity to punishments versus rewards. Biol. Psychiatr. 80, 73–81.
Henriques-Alves, A.M., Queiroz, C.M., 2015. Ethological evaluation of the effects of social defeat stress in mice: beyond the social interaction ratio. Front. Behav. Neurosci. 9, 364.
Hershenberg, R., Satterthwaite, T.D., Daldal, A., Katchmar, N., Moore, T.M., Kable, J.W., Wolf, D.H., 2016. Diminished effort on a progressive ratio task in both unipolar and bipolar depression. J. Affect. Disord. 196, 97–100.
Hodes, G.E., Pfau, M.L., Leboeuf, M., Golden, S.A., Christoffel, D.J., Bregman, D., Rebusi, N., Heshmati, M., Aleysain, H., Warren, B.L., Lebonte, B., Horn, S., Lapidus, K.A., Stelzhammer, V., Wong, E.H.F., Bahn, S., Krishnan, V., Bolanos-Guzman, C.A., Murrough, J.W., Merad, M., Russo, S.J., 2014. Individual differences in the peripheral immune system promote resilience versus susceptibility to social stress. Proc. Natl. Acad. Sci. U. S. A 111, 16136–16141.
Hong, M., Zheng, J., Ding, Z., Chen, J., Yu, L., Niu, Y., Hua, Y., Wang, L., 2012. Imbalance between Th17 and Treg cells may play an important role in the development of chronic unpredictable mild stress-induced depression in mice. Neuroimmunomodulation 20, 39–50.
Hovens, I.B., Nyakas, C., Schoemaker, R.G., 2014. A novel method for evaluating microglial activation using ionized calcium-binding adaptor protein-1 staining: cell body to cell size ratio. Neuroimmunol. Neuroinflammation 1, 82–88.
Iadarola, M.J., Chuang, E.J., Yeung, C.L., Hoo, Y., Silverthorn, M., Gu, J., Draisci, G., 1993. Induction and suppression of proto-oncogenes in rat striatum after single or multiple treatments with cocaine or GBR-12909. NIDA Res. Monogr. 125, 181–211.
Ineichen, C., Sigrist, H., Spinelli, S., Lesch, K.-P., Sautter, E., Seifritz, E., Pryce, C.R., 2012. Establishing a probabilistic reversal learning test in mice: evidence for the processes mediating reward-stay and punishment-shift behaviour and for their modulation by serotonin. Neuropharmacol 63, 1012–1021.
Irifune, M., Nomoto, M., Fukuda, T., 1995. Effects of GBR 12909 on locomotor activity and dopamine turnover in mice: comparison with apomorphine. Eur. J. Pharmacol. 272, 79–85.
Johnson, J.D., Campisi, J., Sharkey, C.M., Kennedy, S.L., Nickerson, M., Greenwood, B.N., Fleshner, M., 2005. Catecholamines mediate stress-induced increases in peripheral and central inflammatory cytokines. Neuroscience 135, 1295–1307.
Kendler, K.S., Karkowski, L.M., Prescott, C.A., 1999. Causal relationship between stressful life events and the onset of major depression. Am. J. Psychiatr. 156, 837–841.
Kim, H., Chen, L., Lim, G., Sung, B., Wang, S., McCabe, M.F., Rusanescu, G., Yang, L., Tian, Y., Mao, J., 2012. Brain indoleamine 2,3-dioxygenase contributes to the comorbidity of pain and depression. J. Clin. Invest. 122, 2940–2954.
Kimura, A., Kishimoto, T., 2010. IL-6: regulator of Treg/Th17 balance. Eur. J. Immunol. 40, 1830–1835.
Kitagami, T., Yamada, K., Miura, H., Hashimoto, R., Nabeshima, T., Ohta, T., 2003. Mechanism of systemically injected interferon-alpha impeding monoamine biosynthesis in rats: role of nitric oxide as a signal crossing the blood-brain barrier. Brain Res. 978, 104–114.
Klaus, F., Paterna, J.-C., Marzorati, E., Sigrist, H., Götze, L., Schwendener, S., Bergamini, G., Jehli, E., Azzinnari, D., Fuertig, R., Fontana, A., Seifritz, E., Pryce, C.R., 2016. Differential effects of peripheral and brain tumor necrosis factor on inflammation, sickness, emotional behavior and memory in mice. Brain Behav. Immun. 58, 310–326.

Klitenick, M.A., DeWitte, P., Kalivas, P.W., 1992. Regulation of somatodendritic dopamine release in the ventral tegmental area by opioids and GABA: an in vivo microdialysis study. J. Neurosci. 12, 2623–2632.
Koob, G.F., Riley, S.J., Smith, S.C., Robbins, T.W., 1978. Effects of 6-hydroxydopamine lesions of the nucleus accumbens septi and olfactory tubercle on feeding, locomotor activity, and amphetamine anorexia in the rat. J. Comp. Physiol. Psychol. 92, 917–927.
Kreisel, T., Frank, M.G., Licht, T., Reshef, R., Ben-Menachem-Zidon, O., Baratta, M.V., Yirmiya, R., 2014. Dynamic microglial alterations underlie stress-induced depressive-like behavior and suppressed neurogenesis. Mol. Psychiatr. 19, 699–709.
Krishnan, V., Han, M.-H., Graham, D.L., Berton, O., Renthal, W., Russo, S.J., LaPlant, Q., Graham, A., Lutter, M., Lagace, D.C., Ghose, S., Reister, R., Tannous, P., Green, T.A., Neve, R.L., Chakravarty, S., Kumar, A., Eisch, A.J., Self, D.W., Lee, F.S., Tamminga, C.A., Cooper, D.C., Gershenfeld, H.K., Nestler, E.J., 2007. Molecular adaptations underlying susceptibility and resistance to social defeat in brain reward regions. Cell 131, 391–404.
Kudryavtseva, N.N., Bakshtanovskaya, I.V., Koryakina, L.A., 1991. Social model of depression in mice of C57BL/6J strain. Pharm Biochem Behav 38, 315–320.
Leventopoulos, M., Russig, H., Feldon, J., Pryce, C.R., Opacka-Juffry, J., 2009. Early Deprivation Leads to Long-term Reductions in Motivation for Reward and 5HT1A Binding and Both Effects Are Reversed by Fluoxetine Neuropharmacology, vol. 56. pp. 692–701.
Liu, X., Zhan, Z., Li, D., Xu, L., Ma, F., Zhang, P., Yao, H., Cao, X., 2011. Intracellular MHC class II molecules promote TLR-triggered innate immune responses by maintaining activation of the kinase Btk. Nat. Immunol. 12, 416–424.
Lu, X.Y., Churchill, L., Kalivas, P.W., 1997. Expression of D1 receptor mRNA in projections from the forebrain to the ventral tegmental area. Synapse 25, 205–214.
Maes, M., 2010. Depression is an inflammatory disease, but cell-mediated immune activation is the key component of depression. Prog. Neuro-Psychopharmacol. Biol. Psychiatry 35, 664–675.
Menard, C., Pfau, M.L., Hodes, G.E., Kana, V., Wang, V.X., Bouchard, S., Takahashi, A., Flanigan, M.E., Aleyasin, H., LeClair, K.B., Janssen, W.G., Labonte, B., Parise, E.M., Lorsch, Z.S., Golden, S.A., Heshmati, M., Tamminga, C., Turecki, G., Campbell, M., Fayad, Z.A., Tang, C.Y., Merad, M., Russo, S.J., 2017. Social stress induces neurovascular pathology promoting depression. Nat. Neurosci. 20, 1752–1760.
Michopoulos, I., Zervas, I.M., Papakosta, V.M., Tsaltas, E., Papageorgiou, C., Manessi, T., Papakostas, Y.G., Lykouras, L., Soldatas, C.R., 2006. Set shifting deficits in melancholic vs. non-melancholic depression: preliminary findings. Eur. Psychiatr. 21, 361–363.
Moransard, M., Sawitzky, M., Fontana, A., Suter, T., 2010. Expression of the HGF receptor c-met by macrophages in experimental autoimmune encephalomyelitis. Glia 58, 559–571.
Nair, A., Bonneau, R.H., 2006. Stress-induced elevation of glucocorticoids increases microglia proliferation through NMDA receptor activation. J. Neuroimmunol. 171, 72–85.
Nilsson, S.R.O., Ripley, T.L., Somerville, E.M., Clifton, P.G., 2012. Reduced activity at the 5HT2C receptor enhances reversal learning by decreasing the influence of the previously non-rewarded associations. Psychopharmacol 224, 241–254.
Nunes, E.J., Randall, P.A., Estrada, A., Epling, B., Hart, E.E., Lee, C.A., Baqi, Y., Muller, C.E., Correa, M., Salamone, J.D., 2014. Effort-related motivational effects of the pro-inflammatory cytokine interleukin 1-beta: studies with the concurrent fixed ratio 5/chow feeding choice task. Psychopharmacology (Berl) 231, 727–736.
Oeckl, P., Lattke, M., Wirth, T., Baumann, B., Ferger, B., 2012. Astrocyte-specific IKK2 activation in mice is sufficient to induce neuroinflammation but does not increase susceptibility to MPTP. Neurobiol. Dis. 48, 481–487.
Ons, S., Rotllant, D., Marin-Blasco, I.J., Armario, A., 2010. Immediate-early gene response to repeated immobilization: fos protein and arc mRNA levels appear to be less sensitive than c-fos mRNA to adaptation. Eur. J. Neurosci. 31, 2043–2052.
Ostrander, M.M., Ulrich-Lai, Y.M., Choi, D.C., Richtand, N.M., Herman, J.P., 2006. Hypoactivity of the hypothalamo-pituitary-adrenocortical axis during recovery from chronic variable stress. Endocrinology 147, 2008–2017.
Pfaffl, M.W., Horgan, G.W., Dempfle, L., 2002. Relative expression software tool (REST) for group-wise comparison and statistical analysis of relative expression results in real-time PCR. Nucleic Acids Res. 30, e36.
Pizzagalli, D.A., 2014. Depression, stress, and anhedonia: toward a synthesis and integrated model. Annu. Rev. Clin. Psychol. 10, 393–423.
Pizzagalli, D.A., Jahn, A.L., O'Shea, J.P., 2005. Toward an objective characterization of an anhedonic phenotype: a signal-detection approach. Biol. Psychiatr. 57, 319–327.
Pryce, C.R., Azzinnari, D., Sigrist, H., Gschwind, T., Lesch, K.-P., Seifritz, E., 2012. Establishing a learned helplessness effect paradigm in C57BL/6 mice: behavioural evidence for emotional, motivational and cognitive effects of aversive uncontrollability per se. Neuropharmacol 62, 358–372.
Pryce, C.R., Fuchs, E., 2017. Chronic psychosocial stressors in adulthood: studies in mice, rats and tree shrews. Neurobiol Stress 6, 94–103.
Rahman, S., McBride, W.J., 2000. Feedback control of mesolimbic somatodendritic dopamine release in rat brain. J. Neurochem. 74, 684–692.
Reinert, K.R., Umphlet, C.D., Quattlebaum, A., Boger, H.A., 2014. Short-term effects of an endotoxin on substantia nigra dopamine neurons. Brain Res. 1557, 164–170.
Rohleder, N., 2014. Stimulation of systemic low-grade inflammation by psychosocial stress. Psychosom. Med. 76, 181–189.
Russo, S.J., Nestler, E.J., 2013. The brain reward circuitry in mood disorders. Nat. Rev. Neurosci. 14, 609–625.
Salamone, J.D., Correa, M., Yohn, S., Lopez Cruz, L., San Miguel, N., Alatorre, L., 2016. The pharmacology of effort-related choice behavior: dopamine, depression, and individual differences. Behav. Process. 127, 3–17.
Salamone, J.D., Pardo, M., Yohn, S.E., Lopez-Cruz, L., SanMiguel, N., Correa, M., 2015. Mesolimbic dopamine and the regulation of motivated behavior. Curr Top Behav Neurosci 27, 231–257.
Savignac, H.M., Finger, B.C., Pizzo, R.C., O'Leary, O.F., Dinan, T.G., Cryan, J.F., 2011. Increased sensitivity to the effects of chronic social defeat in an innately anxious mouse strain. Neuroscience 192, 524–536.
Savitz, J., Drevets, W.C., Smith, C.M., Victor, T.A., Wurfel, B.E., Bellgowan, P.S.F., Bodurka, J., Teague, T.K., Dantzer, R., 2015a. Putative neuroprotective and neurotoxic kynurenine pathway metabolites are associated with hippocampal and amygdalar volumes in subjects with major depressive disorder. Neuropsychopharmacology 43, 463–471.
Savitz, J., Drevets, W.C., Wurfel, B.E., Ford, B.N., Bellgowan, P.S., Victor, T.A., Bodurka, J., Teague, T.K., Dantzer, R., 2015b. Reduction of kynurenic acid to quinolinic acid ratio in both the depressed and remitted phases of major depressive disorder. Brain Behav. Immun. 46, 55–59.
Schmidt, D., Reber, S.O., Botteron, C., Barth, T., Peterlik, D., Uschold, N., Männel, D.N., Lechner, A., 2010. Chronic psychosocial stress promotes systemic immune activation and the development of inflammatory Th cell responses. Brain Behav. Immun. 24, 1097–1104.
Schwarcz, R., Bruno, J.P., Muchowski, P.J., Wu, H.-Q., 2012. Kynurenines in the mammalian brain: when physiology meets pathology. Nat. Rev. Neurosci. 13, 465–477.
Sheng, W., Zong, Y., Mohammad, A., Ajit, D., Cui, J., Han, D., Hamilton, J.L., Simonyi, A., Sun, A.Y., Gu, Z., Hong, J.S., Weisman, G.A., Sun, G.Y., 2011. Pro-inflammatory cytokines and lipopolysaccharide induce changes in cell morphology, and upregulation of ERK1/2, iNOS and sPLA(2)-IIA expression in astrocytes and microglia. J. Neuroinflammation 8, 121.
Sherdell, L., Waugh, C.E., Gotlib, I.H., 2012. Anticipatory pleasure predicts motivation for reward in major depression. J. Abnorm. Psychol. 121, 51–60.
Slavich, G.M., Thornton, T., Torres, L.D., Monroe, S.M., Gotlib, I.H., 2009. Targeted rejection predicts hastened onset of major depression. J. Soc. Clin. Psychol. 28, 223–243.
Slyepchenko, A., Maes, M., Kohler, C.A., Anderson, G., Quevedo, J., Alves, G.S., Berk, M., Fernandes, B.S., Carvalho, A.F., 2016. T helper 17 cells may drive neuroprogression in major depressive disorder: proposal of an integrative model. Neurosci. Biobehav. Rev. 64, 83–100.
Steiner, J., Walter, M., Gos, T., Guillemin, G.J., Bernstein, H.-G., Sarnyai, Z., Mawrin, C., Brisch, R., Bielau, H., Meyer zu Schwabedissen, L., Bogerts, B., Myint, A.-M., 2011. Severe depression is associated with increased microglial quinolinic acid in subregions of the anterior cingulate gyrus: evidence for an immune-modulated glutamatergic neurotransmission? J. Neuroinflammation 8, 94.
Stone, E.A., Lehmann, M.L., Lin, Y., Quartermain, D., 2007. Reduced evoked fos expression in activity-related brain regions in animal models of behavioral depression. Prog. Neuropsychopharmacol. Bol. Psychiatry 31, 1196–1207.
Sublette, M.E., Galfalvy, H.C., Fuchs, D., Lapidus, M., Grunebaum, M.F., Oquendo, M.A., Mann, J.J., Postolache, T.T., 2011. Plasma kynurenine levels are elevated in suicide attempters with major depressive disorder. Brain Behav. Immun. 25, 1272–1278.
Tanaka, K., Furuyashiki, T., Kitaoka, S., Senzai, Y., Imoto, Y., Segi-Nishida, E., Deguchi, Y., Breyer, R.M., Breyer, M.D., Narumiya, S., 2012. Prostaglandin E2-mediated attenuation of mesocortical dopaminergic pathway is critical for susceptibility to repeated social defeat stress in mice. J. Neurosci. 32, 4319–4329.
Treadway, M.T., 2016. The neurobiology of motivational deficits in depression-an update on candidate pathomechanisms. Current Topics in Behavioural Neuroscience 27, 337–355.
Treadway, M.T., Bossaller, N., Shelton, R.C., Zald, D.H., 2012. Effort-based decision-making in major depressive disorder: a translational model of motivational anhedonia. J. Abnorm. Psychol. 121, 553–558.
Treadway, M.T., Zald, D.H., 2011. Reconsidering anhedonia in depression: lessons from translational neuroscience. Neurosci. Biobehav. Rev. 35, 537–555.
Vichaya, E.G., Hunt, S.C., Dantzer, R., 2014. Lipopolysaccharide reduces incentive motivation while boosting preference for high reward in mice. Neuropsychopharmacology 39, 2884–2890.
Wink, D.A., Hines, H.B., Cheng, R.Y., Switzer, C.H., Flores-Santana, W., Vitek, M.P., Ridnour, L.A., Colton, C.A., 2011. Nitric oxide and redox mechanisms in the immune response. J. Leukoc. Biol. 89, 873–891.
Wohleb, E.S., Fenn, A.M., Pacenta, A.M., Powell, N.D., Sheridan, J.F., Godbout, J.P., 2012. Peripheral innate immune challenge exaggerated microglia activation, increased the number of inflammatory CNS macrophages, and prolonged social withdrawal in socially defeated mice. Psychoneuroendocrinology 37, 1491–1505.
Wohleb, E.S., Hanke, M.L., Corona, A.W., Powell, N.D., Stiner, L.M., Bailey, M.T., Nelson, R.J., Godbout, J.P., Sheridan, J.F., 2011. B-adrenergic receptor antagonism prevents anxiety-like behavior and microglial reactivity induced by repeated social defeat. J. Neurosci. 31, 6277–6288.
Wohleb, E.S., McKim, D.B., Shea, D.T., Powell, N.D., Tarr, A.J., Sheridan, J.F., Godbout, J.P., 2014. Re-establishment of anxiety in stress-sensitized mice is caused by monocyte trafficking from the spleen to the brain. Biol. Psychiatr. 75, 970–981.
Wohleb, E.S., Powell, N.D., Godbout, J.P., Sheridan, J.F., 2013. Stress-induced recruitment of bone marrow-derived monocytes to the brain promotes anxiety-like behavior. J. Neurosci. 33, 13820–13833.
Wood, S.K., Wood, C.S., Lombard, C.M., Lee, C.S., Zhang, X.-Y., Finnell, J.E., Valentino, R.J., 2015. Inflammatory factors mediate vulnerability to a social stress-induced depressive-like phenotype in passive coping rats. Biol. Psychiatr. 78, 38–48.
Yang, X.H., Huang, J., Zhu, C.Y., Wang, Y.F., Cheung, E.F., Chan, R.C., Xie, G.R., 2014. Motivational deficits in effort-based decision making in individuals with subsyndromal depression, first-episode and remitted depression patients. Psychiatr. Res. 220, 874–882.